

RESEARCH ARTICLE

WILEY

Glacier thinning, recession and advance, and the associated evolution of a glacial lake between 1966 and 2021 at Austerdalsbreen, western Norway

Gernot Seier^{1,2,3}  | Jakob Abermann² | Liss M. Andreassen⁴ | Jonathan L. Carrivick⁵ | Pål H. Kielland⁶ | Karina Löffler² | Atle Nesje⁷ | Benjamin A. Robson⁷ | Torgeir O. Røthe⁸ | Thomas Scheiber⁸ | Stefan Winkler⁹ | Jacob C. Yde⁸

¹Aeronautical Innovation and Research Laboratories Austria (AIRlabs Austria), Graz, Austria

²Department of Geography and Regional Science, University of Graz, Graz, Austria

³Independent Researcher, Graz, Austria

⁴Norwegian Water Resources and Energy Directorate (NVE), Oslo, Norway

⁵School of Geography and water@leeds, University of Leeds, Leeds, UK

⁶The Norwegian Glacier Museum, Fjærland, Norway

⁷Department of Earth Science, University of Bergen, Bergen, Norway

⁸Department of Environmental Sciences, Western Norway University of Applied Sciences, Sogndal, Norway

⁹Department of Geography and Geology, University of Würzburg, Würzburg, Germany

Correspondence

Gernot Seier, Aeronautical Innovation and Research Laboratories Austria (AIRlabs Austria), Graz 8020, Austria.
Email: gernot.seier@gmx.at

Funding information

The Norwegian Research Council, Grant/Award Number: 302458

Abstract

The Jostedalbreen is the largest ice cap in Norway and mainland Europe. Rapid retreat of many of its outlet glaciers since the 2000s has led to the formation of several glacial lakes. Processes causing the formation and expansion of glacial lakes and their interaction with a glacier and terminal moraine have not been widely addressed yet. In this study, we investigate the degradation of the front of the southeast-facing outlet glacier Austerdalsbreen. Based on a variety of remotely sensed data (UAV-based and airborne orthophotos and DEMs, satellite images), we analyze the coincident glacial and proglacial changes of Austerdalsbreen and quantify the evolution of this transition zone during the last decades. In particular, we focus on the short-term evolution of the glacial lake since 2010, we examine the context of a glacier advance in the 1990s, and we report long-term changes by utilizing 1960s imagery. We discuss the evolution and conditions of Austerdalsbreen compared to other outlet glaciers of Jostedalbreen. Overall, the glacier terminus has experienced a recession in the last decades. The 1990s terminus advance was more restricted than at other nearby outlet glaciers due to glacier surface debris cover, which is a critical factor for the glacier and lake evolution. However, in the most recent period, since 2012, a distinct expansion of a glacial lake is quantifiable. Since the rates of glacier surface lowering also considerably increased since approximately 2017 and the glacier retreated since the beginning of the 2000s with a clear maximum length decrease in 2015, we interpret the recently formed glacial lake as a contributory factor of glacial changes.

KEYWORDS

glacial lake, glacial-proglacial transition, glacier recession and advance, Jostedalbreen, terrestrial photography, unoccupied aerial vehicle and airborne survey

This is an open access article under the terms of the [Creative Commons Attribution-NonCommercial-NoDerivs](https://creativecommons.org/licenses/by-nc-nd/4.0/) License, which permits use and distribution in any medium, provided the original work is properly cited, the use is non-commercial and no modifications or adaptations are made.

© 2023 The Authors. *Land Degradation & Development* published by John Wiley & Sons Ltd.

1 | INTRODUCTION

Worldwide retreat and mass loss of glaciers (Hugonnet et al., 2021; Zemp et al., 2015; Zemp et al., 2020) are indicative of climate change (Thomson et al., 2021). However, while climate change is the dominant driver of glacier mass loss, its spatio-temporal diversity needs to be attributed to local factors. For example, in the European Alps glacier thickness changes vary greatly (Sommer et al., 2020) and those variations can be related to local topography such as elevation and aspect (DeBeer & Sharp, 2009), and to a lesser degree to differences in regional climatic evolution (Abermann et al., 2011). The presence of debris cover and its thickness affects ablation as empirically observed (Østrem, 1959) and described in a theoretical model of glacial melting (Evatt et al., 2015). Due to the water contact of the glacier ice and the related thermally-driven circulation of water in the proglacial water bodies, ice-marginal lakes can be important for glacier ablation and ice dynamics (Carrivick et al., 2022b, 2022c; Carrivick & Tweed, 2013; Truffer & Motyka, 2016).

A precondition for quantifying glacier changes is the use of high-quality and high-resolution data, such as those resulting from photogrammetric surveys (terrestrial, airborne, unoccupied aerial vehicle-based, and archival; for example, Kaufmann & Seier, 2016; Seier et al., 2017; Abermann et al., 2020; Robson et al., 2022), terrestrial and airborne laser scanning (e.g., Abermann et al., 2010), as well as Earth observation satellite data (e.g., Kaufmann et al., 2008) or a combination of techniques (e.g., Fugazza et al., 2018; Seier et al., 2018). The various techniques outlined above emerged at different points in time (e.g., Bhardwaj et al., 2016) and enabled a variety of analyses, for example, compiling glacier inventories and estimating glacier volumes (Andreassen et al., 2015, 2022). Despite pros and cons of each of the techniques, using unoccupied aerial vehicles (UAVs) in protected areas could be critical from a nature conservation perspective, and needs thorough planning (Seier et al., 2021). Recently, high-resolution thermal infrared (TIR) has become increasingly used in glaciology (Tarca & Guglielmin, 2022).

Glaciomorphological features result from various processes, and the characterization of these features is a prerequisite for understanding glacial landforms (Yde et al., 2019). The transformation from glacier-covered to ice-free, proglacial areas is often associated with changes in the glacier surface properties such as debris cover extent and thickness (Fyffe et al., 2020) and supra-glacial lake evolution (e.g., Stefaniak et al., 2021). The presence of thin or thick debris on the glacier surface is the primary factor influencing ablation. Thin debris-covered ice in this context is understood as ice with a supraglacial debris thickness less than a “critical thickness” where surface ablation increases compared to the ablation of clean ice, and is also called “dirty ice” as partially debris-covered ice (Fyffe et al., 2020). Thick debris on the glacier surface exceeds this “critical thickness” and decreases ablation (Østrem, 1959). Debris cover also impacts the structure and seasonal evolution of the glacial drainage system (Fyffe et al., 2019). However, knowledge about debris-covered glacier surfaces over short timescales is limited (Westoby et al., 2020).

Proglacial systems are considered among the most rapidly changing landscapes related to paraglacial processes (Ballantyne, 2002; Carrivick & Heckmann, 2017). The expansion of a glacial lake can

increase ablation rates due to, for example, an increase in the englacial water table, an increase in subglacial water pressure, an increase in the ice surface gradient, favored ice margin flotation, and favored calving (Carrivick & Tweed, 2013). Lake-terminating glaciers show glacier dynamics that is found to be different from land-terminating glaciers (Pronk et al., 2021). This is due to the intensive thermal exchange between lake water and ice, which directly impacts the proglacial evolution (Falatkova et al., 2019). As a result of the current overall mass loss and glacier retreat, the number of ice-marginal lakes is expected to increase (e.g., Carrivick, et al., 2022b). However, ice-marginal lakes are often not explicitly accounted for in studies related to ice loss and glacier dynamics (Carrivick, et al., 2022b; Sutherland et al., 2020).

In Norway, the total glacier area has decreased by ~14% between the former observation period 1999–2006 and the latest inventory of 2018–2019, while the number of glacial lakes has increased (Andreassen et al., 2022). Coincident with glacier area decrease, glacial lakes across Jostedalbreen have increased in number and size (Laute & Beylich, 2021), and the proportions of glacier loss are comparable to those of other glaciers and ice caps in Norway (Carrivick, Andreassen, et al., 2022a). Almost half of the 68 glacial lakes of the Jostedalbreen ice cap are ice-contact lakes (Laute & Beylich, 2021). At Austerdalsbreen, which is part of the Jostedalbreen ice cap, the glacier terminus is characterized by both, overall distinct recession and decay in recent decades interrupted by a short period of advance in the 1990s (Andreassen et al., 2005; Winkler, 2021). The latter period is known as the “Briksdalsbre event” (Nesje & Matthews, 2011), describing the regional glacier advance culminating during the late 1990s in the Jostedalbreen region. From a long-term perspective, the behavior of Austerdalsbreen is in line with the overall retreat of Norwegian glaciers in the 20th century and the observed temporary advances (Andreassen et al., 2005, 2020). However, in the last decade, a glacial lake formed at Austerdalsbreen that converted the land-terminating into a lake-terminating glacier. In the near future, local bedrock topography will lead to the glacier tongue detaching from the lake, provided that retreat continues at Austerdalsbreen.

The aim of this study is to quantify changes in the proglacial area of rapidly changing Austerdalsbreen. We investigate the thinning of the glacier terminus at Austerdalsbreen and the overall evolution of the glacier. Furthermore, we determine the development and subsequent expansion of a recently formed glacial lake and the changes in the glacial-proglacial transition zone in general.

2 | STUDY AREA

Austerdalsbreen is a southeast-facing outlet glacier of Jostedalbreen, the largest ice cap in mainland Europe (Figure 1). The Jostedalbreen is part of the Jostedalbreen National Park in western Norway. Austerdalsbreen drains from the high plateau of Jostedalbreen (1914 m a.s.l.) through two ice falls (Odinsbreen and Thorsbreen) toward the glacier terminus located at 383 m a.s.l. covering a total area of 19.38 km² and a total length of ~8.44 km (Andreassen et al., 2022). The river Austerdalselvi runs along the valley Austerdalen bringing melt water from Austerdalsbreen downstream toward Lake Veitastondsvatnet.

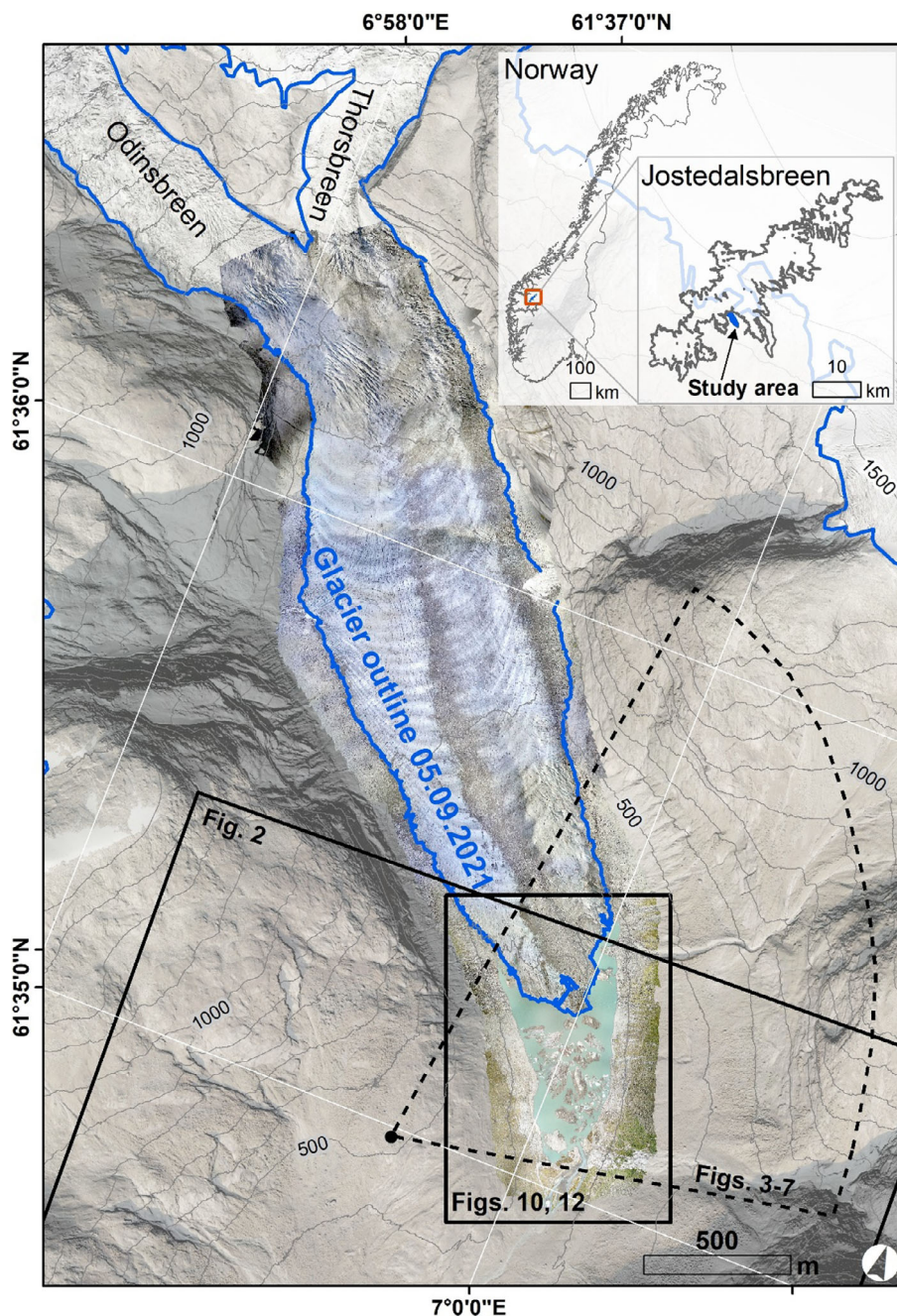


FIGURE 1 Location map of the study area, the lower part of Austerdalsbreen. The blue outline shows the glacier outline in September 2021 and the orthophotomosaic shows results from a UAV-based survey during 3–5 September 2021. The dashed line approximately shows the area covered by annual terrestrial photography since 1991 (approximate photographer's position: black dot). [Colour figure can be viewed at [wileyonlinelibrary.com](https://onlinelibrary.wiley.com/doi/10.1002/ldr.4923)] [wileyonlinelibrary.com](https://onlinelibrary.wiley.com/doi/10.1002/ldr.4923)]

Previous work in the area characterized and described 15 moraine sequences deposited since the Little Ice Age (LIA) until the 1930s in front of Austerdalsbreen (Bickerton & Matthews, 1993). The outermost moraine sequence located ~ 3.2 km down valley represents the LIAs maximum in AD 1786 whereas the AD 1930s moraine sequence lies ~ 1.5 km from the present glacier snout (Bickerton & Matthews, 1993; Erikstad & Sollid, 1986; King, 1959).

3 | DATA AND METHODS

The analysis is mainly based on airborne and UAV-based photogrammetric surveys but also comprises data from airborne laser scanning, satellites, and terrestrial photography (Table 1).

In photogrammetric surveys, signalized objects, for example, target marks used to visualize ground control points (GCPs), that are viewed from a restricted range of angles cause precisions that are significantly reduced along the viewing axis (e.g., Kraus, 1993; Luhmann, 2000). The achievable precision in the viewing direction, σ_z , can be estimated by (Kraus, 1993; Luhmann, 2000).

$$\sigma_z = \frac{\bar{D}^2}{bd} \sigma_i, \quad (1)$$

where \bar{D} is the mean object distance, σ_i is the precision of image measurements (assumed to be a half pixel), b is the distance between the camera centers (i.e., the stereo base), and d is the principal distance of

TABLE 1 Characteristics of the air- and UAV-borne data acquisition along with theoretical precision estimates. Ground sampling distance = GSD.

Acquisition date	Acquired by	Aircraft, camera/scanner	Flying height (m), number of images	Sensor, focal length (mm)	Image size (pixel), pixel size (μm)	GSD, σ_x , σ_z (m)
19./21.07.1966 ^a	Widerøe	Unknown, Wild RC5/RC8	~5800, 7	Photographic film, 152.51	-, 9.4 × 9.4	0.36, 0.54, 1.30
14.08.1986 ^a	Fjellanger Widerøe	Unknown, Wild RC10	~4600, 3	Photographic film, 152.00	-, 9.3 × 9.3	0.28, 0.42, 0.81
25.08.1997 ^a	Fjellanger Widerøe	Unknown, Zeiss RMK Top 15	~4600, 6	Photographic film, 153.603	-, 4.4 × 4.4	0.13, 0.20, 0.37
26.09.2010 ^a	Blom Geomatics AS	Unknown, UltraCam Xp	~4800, 9	CCD, 100.5	17,310 11,310, 6.0 × 6.0	0.29, 0.43, 0.46
25.09.2017 ^a	Terratec	Unknown, UltraCam Eagle	~3800, 17	CCD, 100.5	13,080 × 20,010, 5.2 × 5.2	0.22, 0.30, 0.47
18.08.2020 ^b	Terratec	Piper PA-31 Navajo, Riegl VQ – 1560ii	Unknown, –	–	–	0.50, –, –
03./04./05.09.2021	JOSTICE (UAV)	DJI Matrice 200, Zenmuse XT2	142, 4084	1/1.7" CMOS, 8.00	4000 × 3000, 1.9 × 1.9	0.03, 0.05, 0.12
04.09.2021	JOSTICE (UAV)	Twinfold hexacopter, Sony alpha ILCE-6000	158, 351	APS-C CMOS, 16.00	6000 × 4000, 4.1 × 4.1	0.04, 0.06, 0.12

^aManned aircraft.

^bManned aircraft and airborne laser scanning.

the camera. According to Luhmann (2000), the achievable object precision parallel to the image plane, σ_x ($=\sigma_y$), can be estimated by

$$\sigma_x = m_b \sigma_i, \quad (2)$$

where m_b is the image scale number (calculated by $\frac{\bar{D}_i}{D}$). Considering the intersecting geometry of the imaging configuration, this object precision can be weighted by introducing a design factor q (Fraser, 1996), which can be up to a value of 3 for weak imaging configurations (Luhmann, 2000). In addition to the main survey characteristics, Table 1 also shows the according theoretical precision estimates. Both the survey characteristics and theoretical precision estimates enable to assess of the survey planning and to compare the different data, which shows that the ground sampling distance (GSD) and theoretical estimates of the airborne data are in a similar range, whereas the UAV-based results show lower values by one order of magnitude indicating higher resolution and quality (Table 1).

3.1 | Airborne photogrammetry

Three datasets of historical aerial photographs were used in this study. A survey from 1966 was processed by Terratec (Terratec, 2021). Photogrammetric processing was done based on a bundle block adjustment (BBA). In the first step, a relative orientation was solved using tie points visible in overlapping images. Absolute orientation was implemented using details on stable terrain visible in both the 1966 and 2017 aerial photos. Most parts of the images had good contrast and image matching worked well, thus, only minor manual editing was needed.

The two photographs from 1986 and 1997 were processed within the software Catalyst Professional. The interior orientations were known from calibration reports. The relative and exterior orientations were solved using 108 and 167 tie points and 5 and 4 GCPs for the 1986 and 1997 imagery, respectively. Epipolar images were generated prior to extracting the digital elevation models (DEMs) at 5-m postings using a semi-global matching algorithm, which has been shown to outperform normalized cross-correlation and thereby produce outlier-reduced DEMs (Hirschmüller, 2008).

Linear co-registration biases were removed following the methods presented by Nuth and Käb (2011) implemented through the demcore python module (<https://github.com/dshean/demcore>; Shean et al., 2016) which minimizes the root mean square slope normalized elevation biases over stable terrain. The process was iterated until the standard deviation over stable terrain changed by less than 2%. Upon examining the elevation biases over stable terrain, no non-linear co-registration biases were observed. The DEMs were filtered following the work of Gardelle et al. (2013) where outliers are identified and removed using a threshold of 3 standard deviations of the elevation change over stable terrain per 50-m altitudinal band.

In order to account for hypsometry, the vertical error ($E\Delta v_i$) can be calculated based on the standard error ($E\Delta h_i$) (in m) per 50 m altitudinal band, multiplied by the area of each altitudinal band (A_i) following Bolch et al. (2011) and Gardelle et al. (2013)

$$E\Delta v_i = \sum_i^n E\Delta h_i \times A_i, \quad (3)$$

where $E\Delta h_i$ is derived from the standard deviation over stable ground (σ_{stable}), divided by the effective number of observations (N) (Bolch et al., 2011)

$$E\Delta h_i = \frac{\sigma_{stable}}{\sqrt{N}}, \quad (4)$$

where N is calculated using the number of pixels (N_{tot}) in the DEM differencing, the pixel size (PS), and the distance of spatial autocorrection, d , which we assume to be 20 pixels following Gardelle et al. (2013)

$$N = \frac{N_{tot} \times PS}{2d}. \quad (5)$$

The airborne photographs of 2010 and 2017 were photogrammetrically processed using structure-from-motion and multi-view stereo (SfM-MVS) approaches. The principle of SfM (Ullman, 1979) photogrammetry is that photographs are captured from different perspectives and are subsequently assembled to point clouds using image-matching techniques. The corresponding matching process is based on the identification of interest points and uses the scale-invariant feature transform algorithm (Lowe, 2004). Combined with multi-view stereo techniques, SfM-MVS photogrammetry makes it possible to simultaneously reconstruct dense 3D models, camera positions, and orientations (Brown & Lowe, 2005). The SfM-MVS-photogrammetric approach was implemented using the software Agisoft Metashape (v. 1.5.3). In the first step, data were processed by generating a sparse point cloud followed by a BBA. Finally, a dense point cloud was generated that also included depth filtering. Since the images of frame cameras were used, the interior camera parameters such as focal length, principal point offsets (c_x and c_y), and distortion were fixed according to the calibration protocol. The dense point clouds were exported to orthophotos and DEMs with GSDs of ~ 0.2 – 0.4 m, depending on the respective survey characteristics.

3.2 | Airborne laser scanning

Airborne laser scanning (ALS) was performed on 18 August 2020 as part of establishing the national digital terrain model (DTM) of Norway by the Norwegian mapping authorities. The scanning and data processing was carried out by Terratec AS (Terratec, 2020). As the scanning is performed over several days snow and ice melting may cause differences in surface elevation within the same resulting scene. The scanning was performed at a resolution of a minimum of 2 points/m² with a Riegl VQ-1560ii instrument and resulted in a DTM with 0.5 m GSD (Table 1).

3.3 | UAV-based photogrammetry

3.3.1 | UAV-based survey 2021

UAV-based surveys at Austerdalsbreen were conducted between 3 and 5 September 2021 using two different multirotor solutions

(Table 1). It required 10 flights to cover the entire area of interest resulting in ~ 4400 photographs that were captured in the visible spectrum using user-grade cameras (Table 1). In terms of georeferencing, both, direct and indirect approaches were used, which is why signalized objects were geodetically measured using the Global Navigation Satellite System (GNSS). The weather conditions were favorable to the flights throughout the three survey days with low wind speeds and good visibility.

3.3.2 | Processing and analysis of orthophotomosaics, DEM, and thermal imagery

The processing of the UAV-based photographs in the visible spectrum was implemented using the SfM-MVS photogrammetry approach outlined in Section 3.1. However, since in this case, amateur cameras were used, a Sony alpha 6000 and a DJI Zenmuse XT2, the camera parameters such as focal length, principal point offsets (c_x and c_y), and radial distortion were set to adjustable in the process of camera self-calibration. The georeferencing was implemented using an integrated approach, combining GCP measurements with post-processing kinematics-based direct measurements of sensor positions. The dense point clouds were exported to an orthophotomosaic with a GSD of 0.05 m and to a DEM with a GSD of 0.09 m.

In addition, one of the cameras used (the DJI Zenmuse XT2) also includes a thermal sensor, a Forward Looking Infrared, which is sensitive in the long-wave infrared (7.5–13.5 μm). The TIR images were acquired on 5 September 2021. Considering the emission of the target object (E_{obj}), the emission of the surroundings, reflected by the object (E_{refl}), and the emission of the atmosphere (E_{atm}), the radiation received by a camera (W_{tot}) can be described using the following equation (Herreid, 2021; Usamentiaga et al., 2014):

$$W_{tot} = \varepsilon_{obj} \tau_{atm} \sigma^* (T_{obj})^4 + (1 - \varepsilon_{obj}) \tau_{atm} \sigma^* (T_{refl})^4 + (1 - \tau_{atm}) \sigma^* (T_{atm})^4, \quad (6)$$

where ε_{obj} is the emissivity of the object, τ_{atm} is the transmittance of the atmosphere, T_{refl} (K) is the reflected temperature, T_{atm} (K) is the temperature of the atmosphere, σ is the Stefan-Boltzmann constant ($5.67 \times 10^{-8} \text{ Wm}^{-2} \text{ K}^{-4}$), and T_{obj} (K) is the surface temperature of an object. The surface temperature can thus be calculated following Usamentiaga et al. (2014):

$$T_{obj} = W_{tot} - (1 - \varepsilon_{obj}) \tau_{atm} \sigma^* (T_{refl})^4 - (1 - \tau_{atm}) \sigma^* (T_{atm})^4 \quad \varepsilon_{obj} \tau_{atm} \sigma^* \quad (7)$$

Accordingly, the TIR images were used to deduce surface temperatures. Apart from σ , none of these quantities are constant. The emissivity used in the calculation for debris and debris-covered ice followed the suggestions and practice of Aubry-Wake et al. (2015), Kraaijenbrink et al. (2018), and Herreid (2021) and was set to 0.94, to 0.97 for clean ice, and to 0.98 for water.

3.4 | Time-series analysis of the lake extent

To assess the evolution of the glacial lake, a series of satellite images (Sentinel-2, Landsat 5, Landsat 7, Landsat 8, and ASTER) acquired during the months of July or August (since 2010) were used. In the first step, the lake area was determined manually using the Google Earth Engine Digitisation Tool (GEEDiT) (Lea, 2018). In a second step, lake area changes were calculated between each of the consecutive years using the function “symmetric difference” in QGIS. The time range of the acquisition varied within the summer months throughout the different satellite-based products (see Section 5.2). In addition, we used orthophotosmosaics of airborne and UAV-based surveys in 2010, 2017, and 2021 (Table 1) for delineating the lake area.

3.5 | Terrestrial photography

During the early 1990s and in the context of various research activities, one of the authors, Stefan Winkler, started a still ongoing visual glacier front monitoring at multiple outlet glaciers of Jostedalbreen. Standard Single-Lens Reflex cameras were used to annually (partly bi-annually) obtain photographs from almost identical positions on the selected glacier forelands (Winkler, 2008; see also: glacier.nve.no/viewer/GPP/no; Figure 1). Although Austerdalsbreen could not be visited every year, it is worth mentioning that especially the period of advance in the 1990s has been covered very well (see Section 4.2). Images taken on conventional color slide film roll have meanwhile been scanned.

4 | GLACIER CHANGES

4.1 | Post-LIA changes

Despite a lack of direct historical evidence allowing precise dating, Austerdalsbreen had its maximum LIA extent during the mid- or late-18th century CE, that is, synchronous to other outlets of Jostedalbreen (Nesje et al., 2008). The most reliable date for the LIA maximum is 1761–95, presented by Bickerton and Matthews (1993) using detailed lichenometric studies (Figure 2a). The high number of terminal moraines representing short-term re-advances on the foreland of Austerdalsbreen shows that the subsequent retreat from the LIA maximum position was interrupted by short-term frontal oscillations. Some of these moraines may potentially be linked to seasonal advances during periods of stationary or slowly retreating glacier margins (King, 1959; Winkler, 2021). The flat and broad outer part of the glacier foreland is to a large extent dominated by glaciofluvial deposits, and the abovementioned moraine ridges are intersected by the river. The changes in the river channels do not necessarily show a chronological connection to nearby moraine ridges as Maizels and Petch (1985) and Petch and Whittaker (1997) demonstrated in their lichenometric studies. After the 1930s, the glacier front receded through an area where the valley bends from a N-S to a NW-SE

orientation, and a bedrock riegel causes a narrowing of the glacial river plain. This may have led to a lack of distinct moraine ridges between the 1930s and 2000.

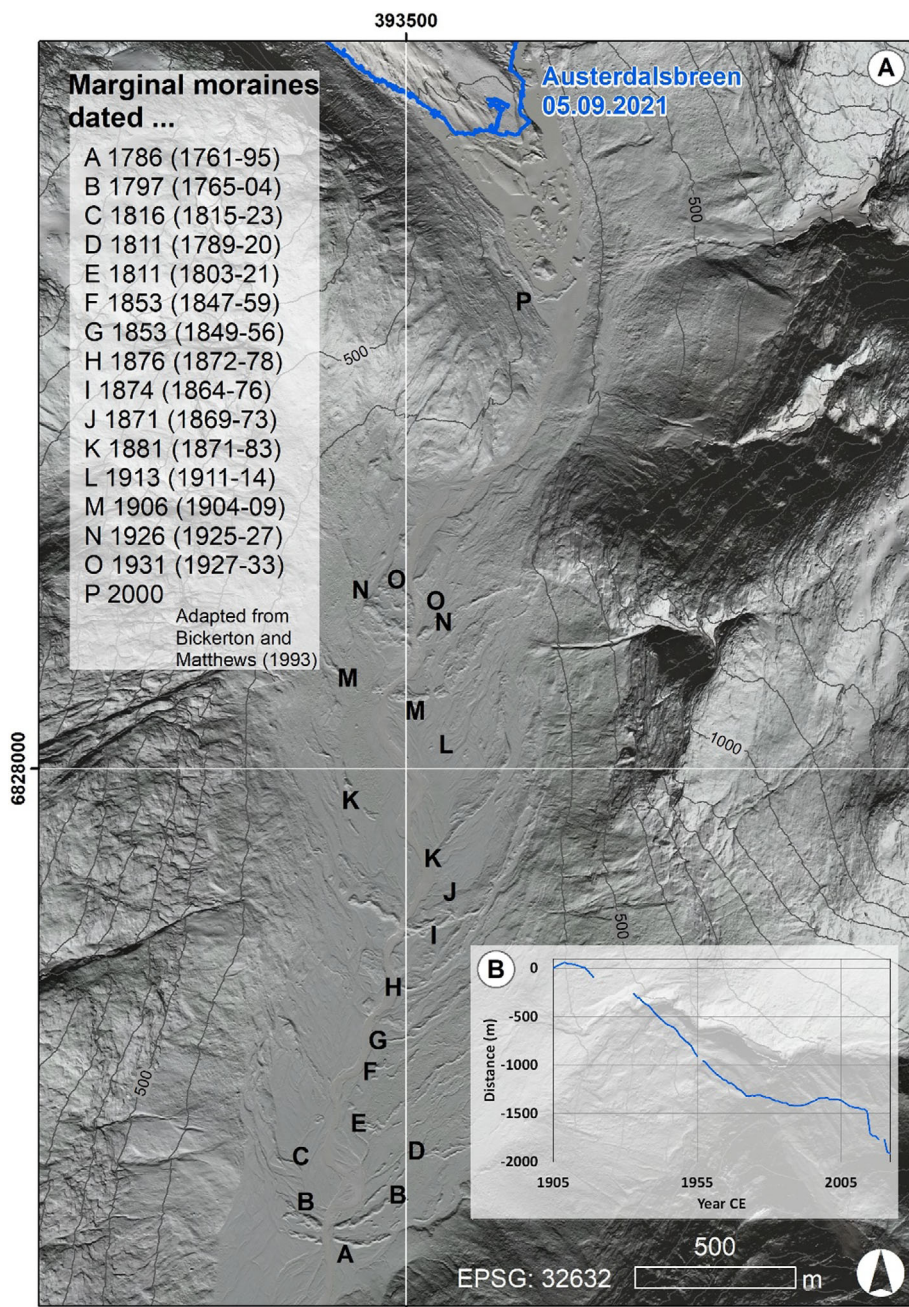
Front variation has been measured on Austerdalsbreen since 1905 from fixed landmarks to the glacier terminus in a defined direction to be representative for glacier length changes (Kjøllmoen et al., 2022; Rekstad, 1906). Typically, one data point has been used to measure the front variation and length change each year. Figure 2b shows a small advance in the first years, a continuous retreat from the 1930s to the 1960s, and then a small advance in the mid-1970s and a larger advance in the 1990s before the glacier started to retreat from the 2000s (NVE, 2022; Rekstad, 1906). The net retreat from 1905 to 2022 is 1.9 km (NVE, 2022).

4.2 | The glacier advance in the 1990s

Austerdalsbreen advanced in the 1990s during the so-called “Briksdalsbreen event.” With a total length change of +82 m between 1991 and 2000 (NVE, 2022) this advance was, however, considerably less than at other Jostedalbreen outlet glaciers (Andreassen et al., 2005; Winkler et al., 2009). Around Jostedalbreen, the “Briksdalsbreen event” resulted in the formation of terminal moraines on the inner glacier forelands with ice pushing and bulldozing of unconsolidated proglacial sediments by the advancing glaciers as the dominant process (for details see Winkler & Nesje, 1999; Winkler & Matthews, 2010; Winkler, 2021). Geomorphological processes related to the glacier advance at Austerdalsbreen were different and more complex due to the specific conditions at its lowermost glacier tongue at this time responsible for those minor total length changes.

At the onset of the “Briksdalsbreen event” in 1991–1992 (Figure 3a), the geomorphological situation at the terminus of Austerdalsbreen was characterized by a large, extensively debris-covered complex of stagnant ice (Figure 4a). It was physically still connected to the active lower glacier tongue but otherwise initially showed similarities with ablation moraines as, for example, described by Bennett and Glasser (2009). This debris-ice complex showed several ice-disintegration features and was surrounded by a proglacial pond that was covered by the advance in the early 1990s (Figure 4b,d). At the terminus of Austerdalsbreen the active part of the lower glacier tongue was advancing into this stagnant debris-ice complex and exhibiting considerable pressure on it (Figure 3). In turn, the static, motionless debris-ice complex acted as an obstacle for any expansion of the active part of the glacier tongue. As a consequence, the debris-ice complex clearly shrank already by 1995 and was completely modified (practically overridden and integrated into the active tongue) in the course of the advance. In around 2000, the active glacier front was in a similar position as the debris-ice complex had around 1990 (Figure 4f).

Likely due to tensions caused by the debris-ice complex acting as an obstacle for the expanding and faster-moving advancing active glacier tongue, prominent shear planes were observed at its southwestern latero-frontal section where the glacier surface had risen and exhibited a typical convex shape (e.g., Figure 3c). These shear planes



could easily be visually traced and considerable quantities of englacial debris were melting out at some of them. Below, those shear plane deposition of that englacial and supraglacial debris caused the formation of a few ice-sceer fans along the latero-frontal glacier margin (Figure 4c). Those were, however, short-lived as ongoing latero-frontal expansion during the second half of the 1990s modified and subsequently destroyed these features as well as small latero-frontal moraine ridges that had been formed before the advance (Figure 4e). First, in 1996, a small moraine ridge encircling the remaining down-valley part of the debris-ice complex gave evidence that the active glacier tongue finally had exerted control over the former (Figure 3d). This moraine ridge consisted of predominately sandy sediment of glaciofluvial origin deposited in the former glacial lake and its feeding

marginal meltwater streams. Genetically, it was a typical push moraine similar to contemporary moraines at other glaciers in the region (see above), but already since 2001, this sandy moraine deteriorated quickly as a consequence of further advances and its less compact, unstable sedimentological properties (Figure 4f).

4.3 | Austerdalsbreen in the 2000s

The advance ceased by the end of the 1990s and left Austerdalsbreen with a debris-covered front. In the following years, down-wasting and back-wasting processes (Krüger & Kjær, 2000) dominated the melting of the debris-covered front, while glacier ice

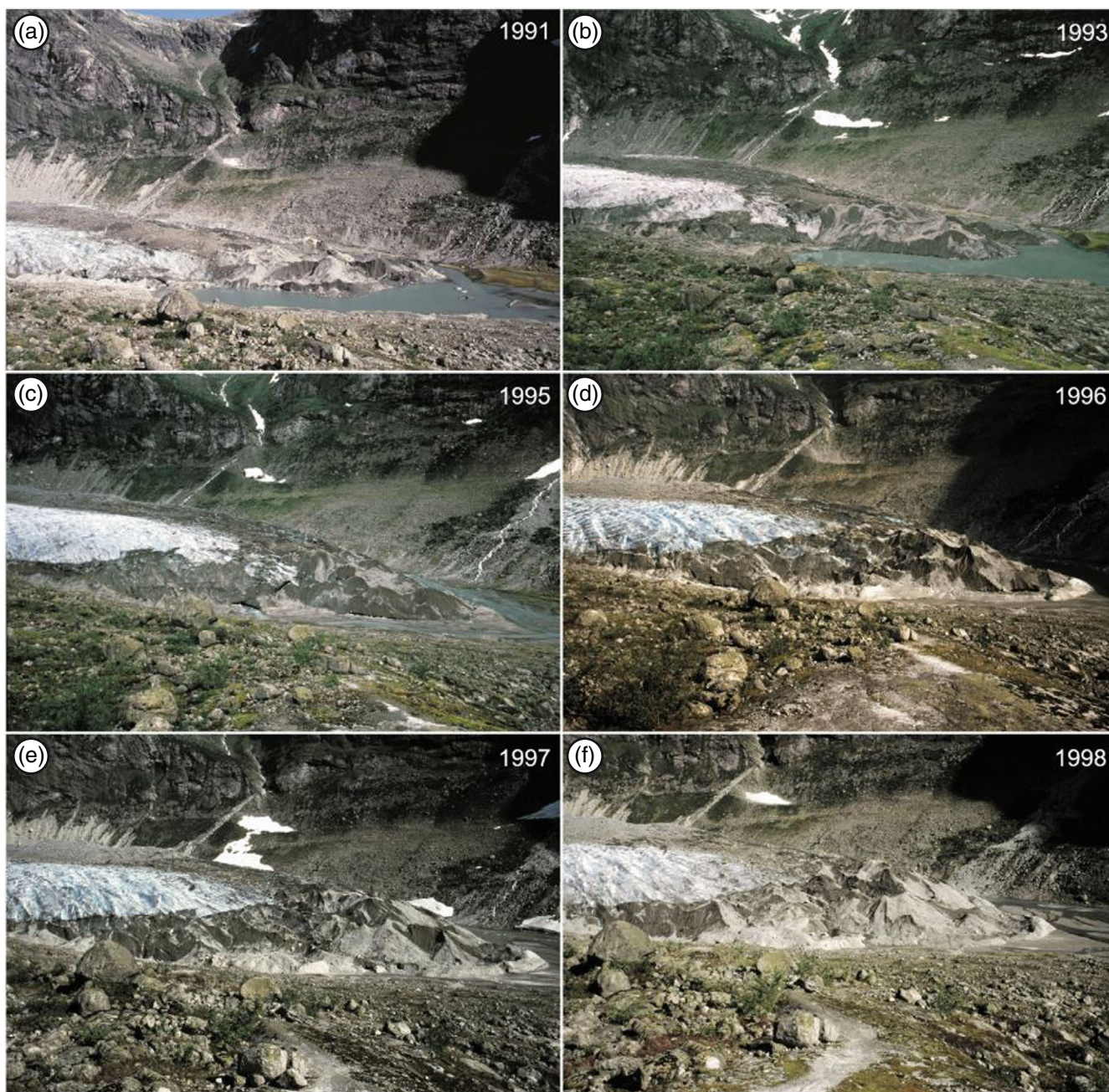


FIGURE 3 View of the central lower glacier tongue of Austerdalsbreen: (a) 31.08.1991; (b) 12.08.1993; (c) 24.08.1995; (d) 21.08.1996; (e) 17.08.1997; and (f) 03.09.1998. The advance of Austerdalsbreen during this period resulted in a visible thickening of the debris-covered glacier tongue and final disappearance of the proglacial lake in 1996. Photographs: Stefan Winkler. [Colour figure can be viewed at [wileyonlinelibrary.com](https://onlinelibrary.wiley.com/doi/10.1002/ldr.4923)]

exposed up-glacier of the uppermost debris-rich shear band melted at a faster rate than the debris-covered front (Figure 5). This albedo-induced deviation in melt rates caused lateral retreat of the near-vertical ice slope behind the uppermost shear band, forming a depression between the debris-covered front and the cleaner glacier ice. As shown in the time series in Figure 5, this depression became progressively dirtier as sediment from both the debris-covered front and the medial moraine was washed into the depression. It is also worth noting that through the 2000s, the terminal part of the debris-

covered front was only affected by limited down-wasting and became more stable because of increasing debris cover and less exposure of its ice core. This is evident by the light grey color of the debris cover in Figure 5.

The difficulties in distinguishing between stagnant debris-covered ice at the front and active glacier ice further up-glacier caused challenges in objectively defining the location of the active glacier terminus and thus to measure glacier recession. Also, the lateral parts of the front melted faster than the central part (Figure 5). The glacier

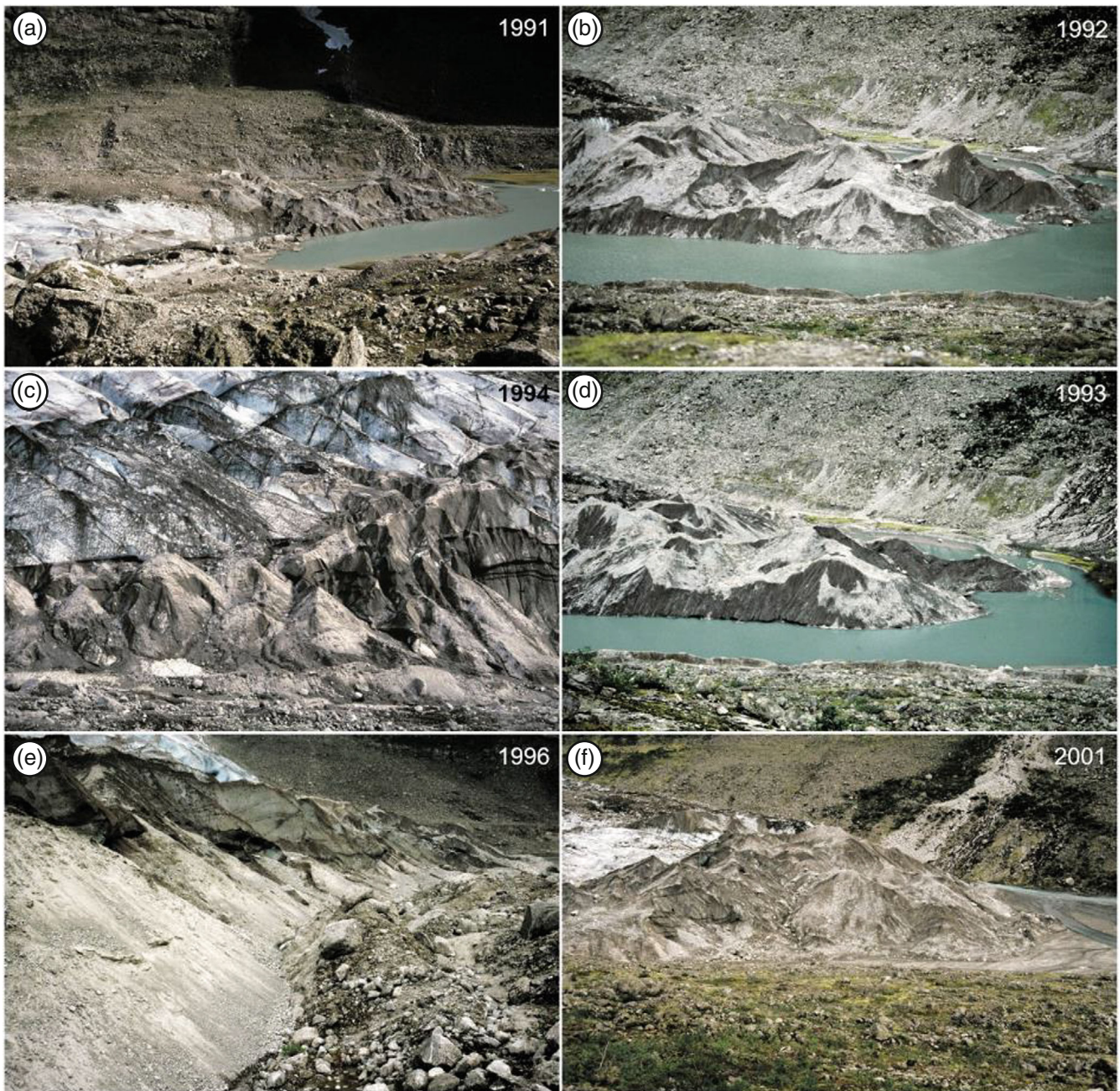


FIGURE 4 Morphological processes at the terminus of Austerdalsbreen during the recent advance in the 1990s: (a) Active lower glacier tongue (right) and static down-valley complex of stagnant ice and debris (left), 31.08.1991; (b) Debris-ice complex on 11.08.1992; (c) Prominent shear planes and ice-scree fans along the latero-frontal margin, 08.08.1994; (d) Debris-ice complex on 12.08.1993—note the development of ice-disintegration features and local expansion of a glacial pond in comparison to (b); (e) Ice overriding remnants of ice-scree fans and (subsequently) older latero-frontal moraines, 21.08.1996; and (f) View of the frontal glacier margin showing the final stage of development of the former debris-ice complex when the advance ceased, 29.08.2001 (note that photos (c) and (e) are taken from lower positions slightly up-glacier. Photographs: Stefan Winkler. [Colour figure can be viewed at wileyonlinelibrary.com]

front record (Figure 2b) shows that from autumn 2000 to autumn 2001 Austerdalsbreen retreated 20 m, the first retreat on record since the 1980s. A 5 m advance was recorded the year after, but from 2003 to 2010 the terminus position retreated 92 m. However, the central part of the stagnant debris-covered front only retreated 10–20 m during this decade.

4.4 | Recession and thinning of Austerdalsbreen after 2010

Austerdalsbreen continued to thin and retreat after 2010. The first observation of periodic flooding within the extent of the 1990s advance was in 2011 (Figure 6a) where a small outwash plain had

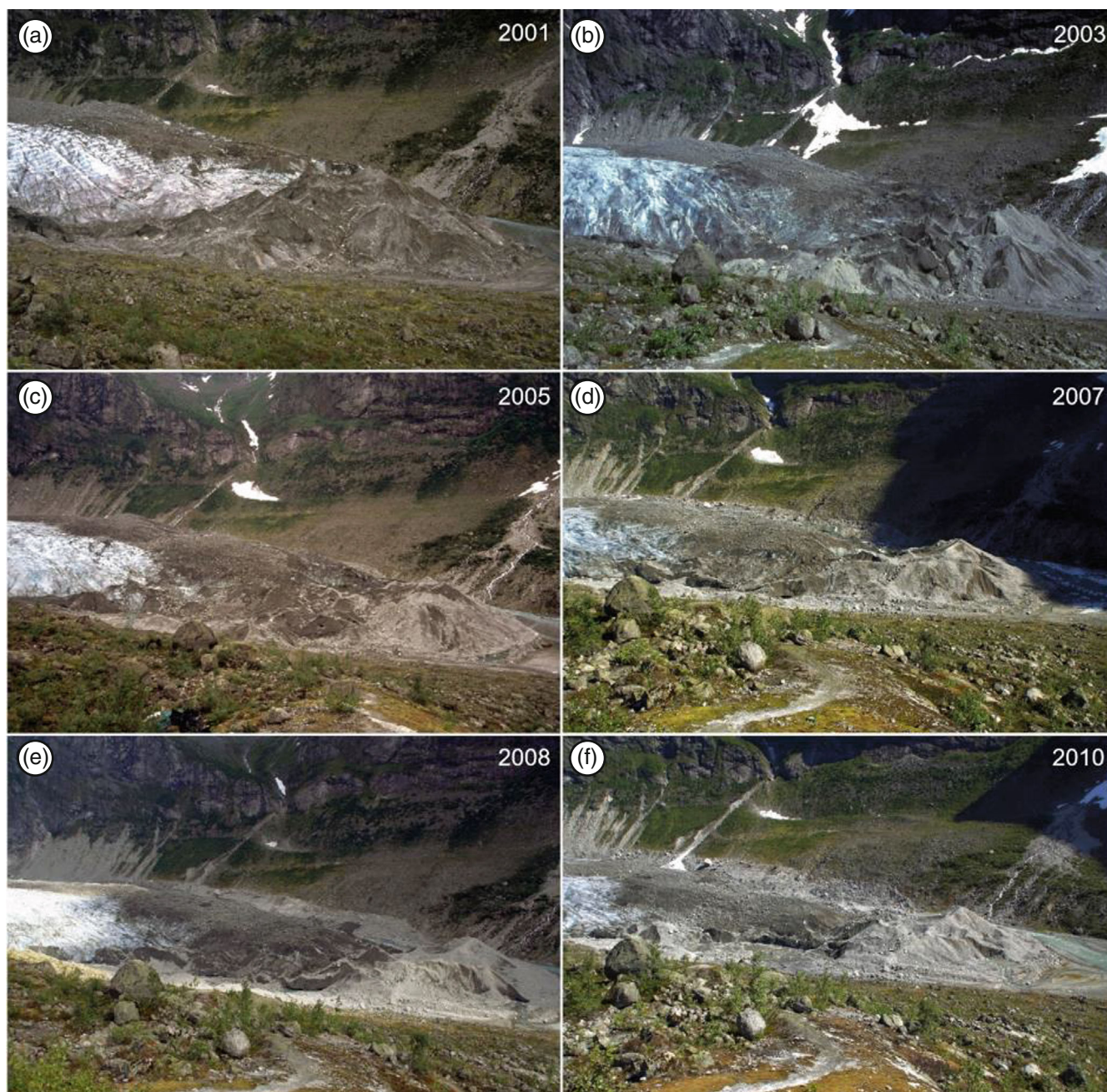


FIGURE 5 View of the central lower glacier tongue of Austerdalsbreen in the 2000s: (a) 29.08.2001; (b) 26.06.2003; (c) 19.08.2005; (d) 22.08.2007; (e) 24.08.2008; and (f) 01.07.2010. The glacier front thinned significantly during this period. Debris that originally derived from the medial moraine or the most distal shear band spread over a larger area of the former clean ice glacier surface as a consequence of higher ablation of the clean ice and back-wasting of the debris-covered front. Photographs: Stefan Winkler. [Colour figure can be viewed at [wileyonlinelibrary.com](https://onlinelibrary.wiley.com/doi/10.1002/ldr.4923)]]

formed along the southern part of the front. This area was not inundated in 2012 and 2013 (Figure 6b,c). In 2014–2015, the stagnant debris-covered front was largely detached from the active glacier ice above surface level, and several ponds and lakes became permanent, although very dynamic, landform features (Figure 6d,e). Below the surface, the debris-covered front was still attached to active glacier ice. Thus, the ponds and lakes should be characterized as supraglacial features. In the following years (Figure 6e,f; Figure 7), the degradation of the debris-covered front continued, and ponds and lakes merged into large units and the total lake area increased.

From autumn 2010 to autumn 2020, the total retreat recorded was 327 m (Figure 2b). The largest single-year retreat was from autumn 2014 to autumn 2015 with a retreat of 225 m due to the superficial detachment of the debris-covered front. The measurements after 2015 were then continued for the front of the active glacier ice. A large annual retreat was also recorded from autumn 2020 to autumn 2021 with a retreat of 130 m. However, these glacier recession rates should be considered as very rough estimates, as terminus measurements were challenging in these years due to the uneven terminus, which can result in highly variable results depending on the chosen line of sight or flowline.

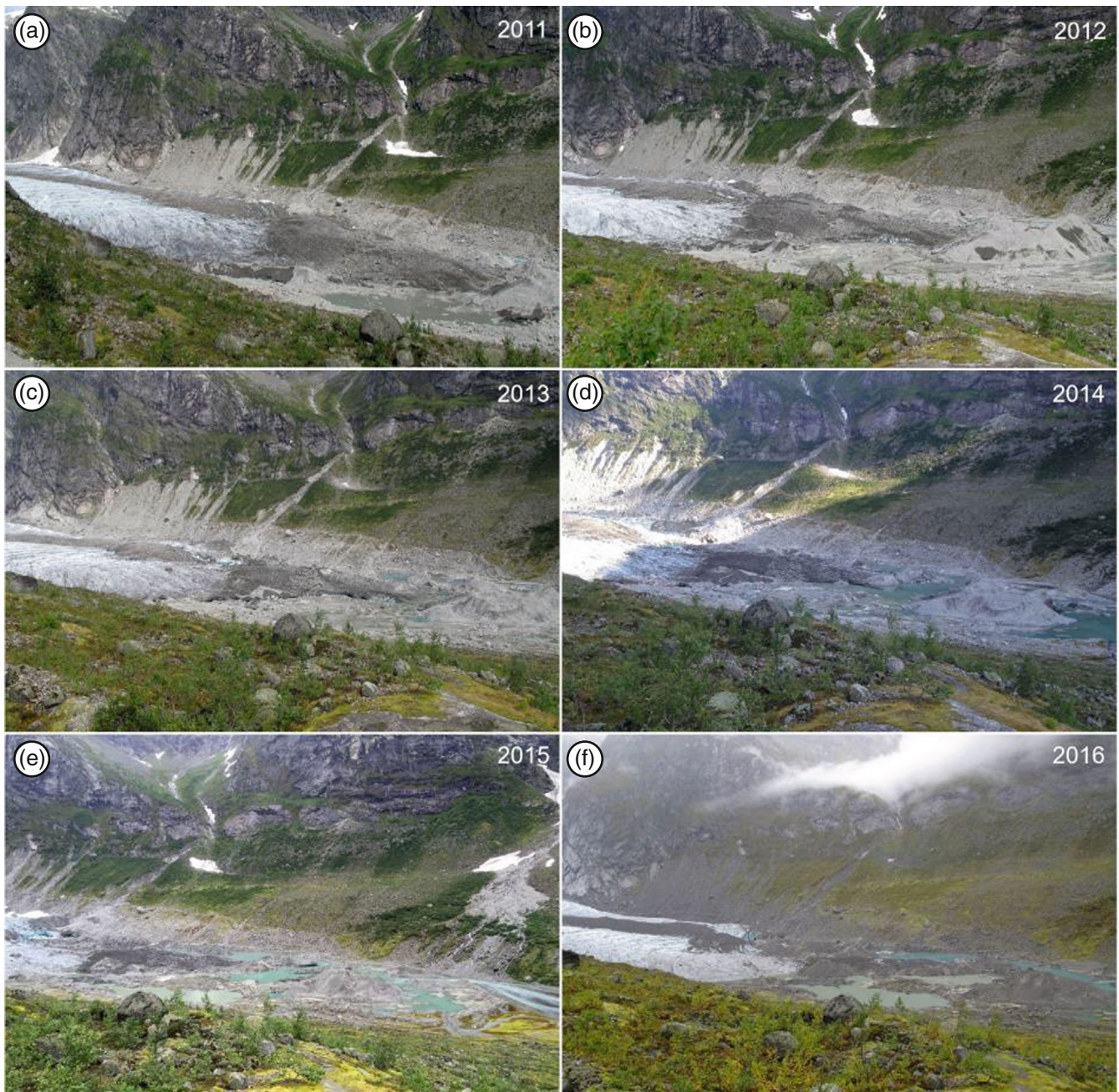


FIGURE 6 Degradation of the glacier front of Austerdalsbreen 2011–2016: (a) 28.07.2011; (b) 08.08.2012; (c) 29.08.2013; (d) 09.08.2014; (e) 17.09.2015; and (f) 24.09.2016. The first signs of formation of a new glacial lake started to show during this period. In 2014–2015, the frontal ice-cored moraine was detached from the active glacier ice. Photographs: (d) Per Solnes, all other photographs by Jacob C. Yde. [Colour figure can be viewed at [wileyonlinelibrary.com](https://onlinelibrary.wiley.com/doi/10.1002/ldr.4923)]

5 | RESULTS

5.1 | Glacier surface lowering and glacier change rates

5.1.1 | Quality assessment

When using GCPs, the quality of photogrammetric reconstruction is in the range of a few centimeters for the UAV-based survey, a few

decimeters for recent airborne surveys and amounts to ~ 1 m for archival airborne photographs, taking root-mean-square errors (RMSEs) into consideration, irrespective of the survey characteristics (Table 2). This applies to both the planimetric (XY) and elevation (Z) values. Besides photogrammetric processing, independent check points (ICPs) enable us to assess the vertical quality of the 2021 DEM based on standard deviation (SD), which is in the range of a few decimeters, and based on a mean value of 0.36 m (Table 2). The SDs and RMSEs of the ICPs are in the same range and thus independently

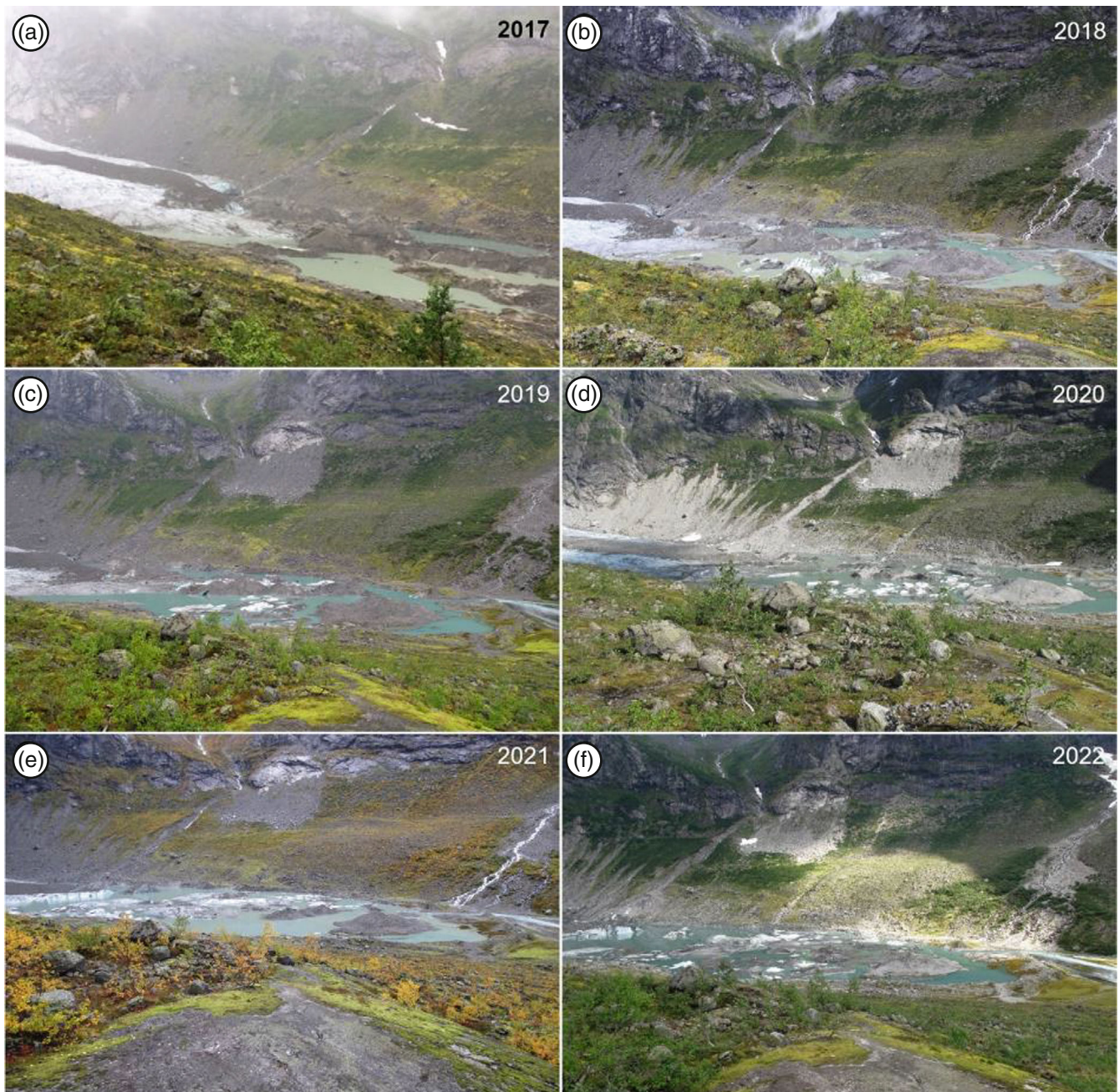


FIGURE 7 Formation of a new glacial lake at Austerdalsbreen 2017–2022: (a) 08.10.2017; (b) 23.08.2018; (c) 22.08.2019; (d) 20.08.2020; (e) 27.09.2021; and (f) 24.08.2022. Ponds and small lakes gradually merged into a larger glacial lake with debris-covered “ice-cored” islands. Photographs: (a) Per Solnes, (b) Marthe Gjerde, (c–f) Jacob C. Yde. [Colour figure can be viewed at [wileyonlinelibrary.com](https://onlinelibrary.wiley.com/terms-and-conditions)]

confirm the high quality of the 2021 DEM. From a methodological point of view, we would in this case (2021 DEM) expect elevation differences in the range of a few centimeters. Nevertheless, comparison to GNSS measurements mounted on a backpack is only to a limited extent useful for validation as the approach itself holds an inherent uncertainty in the range of a few decimeters.

Other than that, in traditional photogrammetry, it is good practice to relate the theoretical estimate σ_z to the survey range, which results in relative precision ratios. In our case, these ratios are comparable to those usually achieved ($\sim 1:1000$) in both SfM-MVS-based and

traditional photogrammetry (James & Robson, 2012) and vary between 1:1140–1:12300 (Table 2). The accuracy ratios, which result from relating the RMSEs to the survey range, vary between 1:1800 and 1:14600 (Table 2) and are indicative of similar or even better qualities than we would expect from other SfM-MVS-based studies (Smith & Vericat, 2015). Our results can therefore be considered precise and accurate.

Considering the different data used, the vertical error (see Section 3.1) of DEMs assessed at stable ground was in a range of a few centimeters per year (Table 3).

TABLE 2 Quality of the photogrammetric processing and DEMs based on ground control points (GCPs) and independent checkpoints (ICPs), as well as relative precision ratios and accuracy ratios.

Acquisition date	GCP XY RMSE (m) ^a	GCP Z RMSE (m) ^a	GCP image plain RMSE (px) ^a	Vertical quality, ICP SD (m) ^b	Vertical quality, ICP RMSE (m) ^b	Vertical quality, ICP mean (m) ^b	Relative precision ratio ^c	Accuracy ratio ^d
19./21.07.1966	0.55 (38)	0.52 (38)	Not reported	-	-	-	~1:4500	~1:10500
14.08.1986	0.66 (23)	0.19 (23)	1.57 (23)	-	-	-	~1:5700	~1:7000
25.08.1997	2.61 (4)	0.48 (4)	1.15 (4)	-	-	-	~1:12300	~1:1800
26.09.2010	0.36 (6)	0.08 (6)	0.4 (6)	-	-	-	~1:10400	~1:13000
25.09.2017	0.26 (6)	0.24 (6)	0.7 (6)	-	-	-	~1:8000	~1:14600
03./04./05.09.2021	0.05 (27)	0.07 (27)	1.6 (10)	0.31 (12445)	0.48 (12445)	0.36 (12445)	~1:1140	~1:1800

Abbreviations: px, pixel; RMSE, root means square error; SD, standard deviation.

^aBased on GCPs, number of points in parentheses.

^bBased on ICPs, number of points in parentheses.

^cThe ratio of the theoretical estimate σ_z to \bar{D} .

^dThe ratio of the RMSE to \bar{D} .

TABLE 3 Vertical error of DEMs assessed at stable ground.

Period of time	Vertical error (m a ⁻¹)
1966–1986	0.03
1986–1997	0.02
1997–2010	0.03
2010–2017	0.04
2017–2020	0.05
2020–2021	– ^a

^aNot enough stable ground covered in the respective DEMs to perform a calculation.

5.1.2 | Elevation differences and glacier change rates

Our data reveal that the glacier tongue of Austerdalsbreen has thinned in the observation period 1966–2021 (Figures 8 and 9). Throughout the six subperiods, the glacier surface lowering is marked by increased change rates (Figure 8, Table 4; note that the time intervals and the areas used in the calculations differ), with some minor exceptions in the upper, that is, north-western section of the glacier tongue. Most notably, the glacier terminus has been lowering at an accelerated rate since the 1960s amounting to up to ~ -20 m a⁻¹ in the period 2020–2021 (Figure 10, Table 4). While the change rates of the glacier tongue are spatially heterogeneous throughout the periods 1966–2010, in the periods since 2010 the change rates are rather spatially homogeneous at an increasing rate. By comparing the mean glacier elevation change rates of the subperiod 2010–2021 with those of the entire period 1966–2021 (Table 4), the onset of increased surface lowering since 2010 is deducible. Increased rates of glacier surface lowering especially affecting the glacier front have been recognizable since 2010 (Figure 10). Similarly, the glacier volume has decreased throughout the observation period at an increased rate since 2010 (Table 4).

5.2 | Formation of the lake and areal changes

The glacial lake formed as a permanent landform in 2014, although smaller ponds and inundated outwash plains were observed in previous years. Between 2010 and 2021, the total area of the lake at Austerdalsbreen increased from ~ 0.008 km² in 2010 to ~ 0.1 km² in 2021 (Figure 11). The increase in the glacial lake's area appears almost linear irrespective of the data used and developed from 2012 and 2013 with a water-covered area of ~ 0.01 and ~ 0.02 km², respectively (Figure 11).

6 | DISCUSSION

6.1 | Surface temperature conditions during the 2021 UAV-based survey

From a TIR measurement, we found that the water temperature of the glacial lake is a constant source of heat energy compared to the clean ice (Figures 12 and 13). The ice surface characteristics play a vital role here too, which is expressed in the clearly higher surface temperatures of debris-covered ice compared to clean ice (Figure 13), even though a clear differentiation of surface temperatures of dirty ice and thick debris-covered ice is not possible. Debris-covered land, however, shows by far the highest surface temperatures. During the TIR survey (on 5 September 2021) partly cloudy conditions prevailed, which is why insolation likely did not impact the measurement significantly.

6.2 | Interaction between ice ablation rates, lake formation, damming by the terminal moraine, and debris-covered glacier ice

The foreland of Austerdalsbreen, between its LIA maximum position and the inner bedrock sill, which is the glacier margin position during

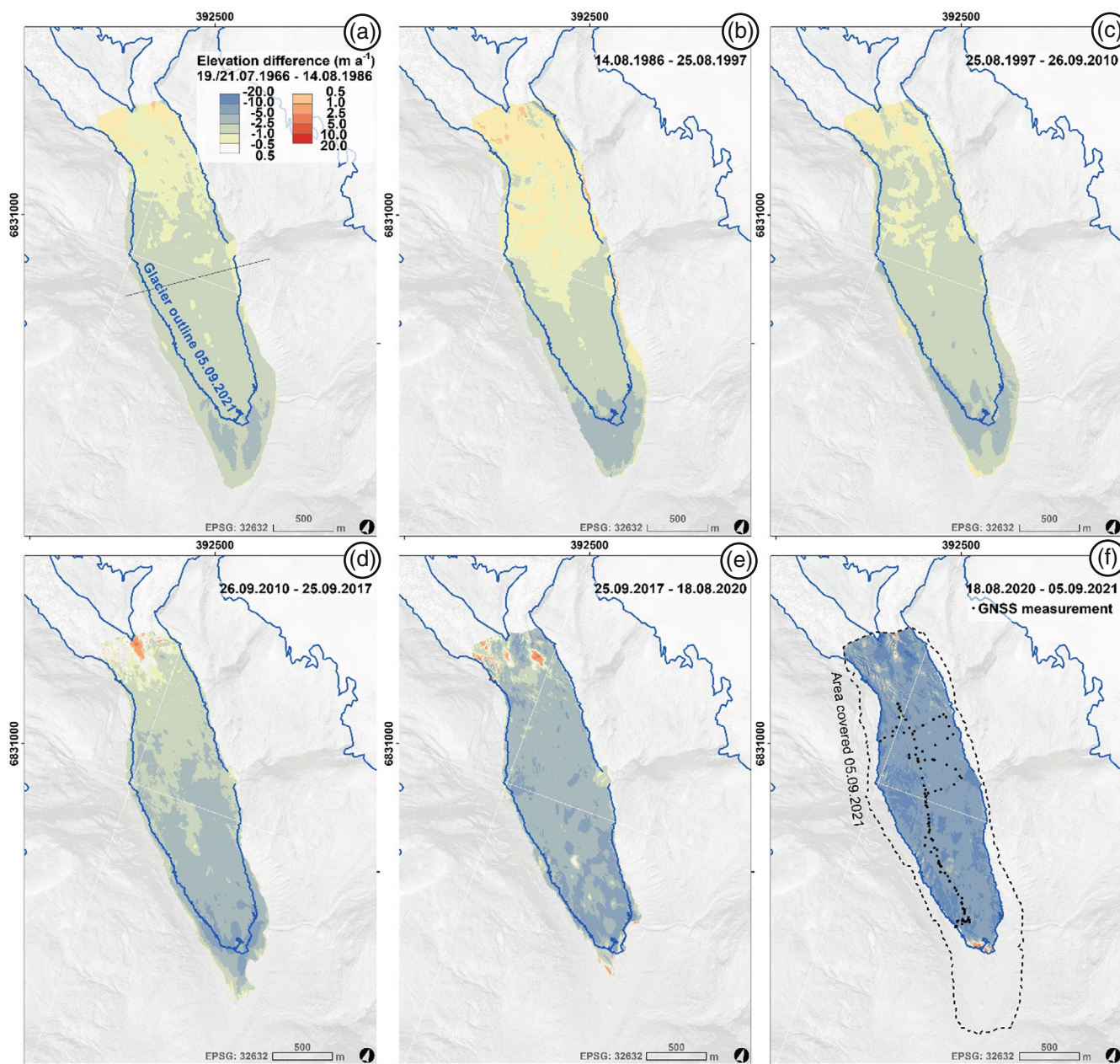


FIGURE 8 Maps showing elevation differences throughout the observation period at Austerdalsbreen. Note that the presented elevation differences are based on different time intervals. The glacier outline of September 2021 is shown in all images (blue line). The upper limit of the area compared is based on the extent of the data acquisition in 2021 (dashed line in (f)). The straight grey line in (a) shows the location of the cross-sectional profile presented in Figure 9. [Colour figure can be viewed at [wileyonlinelibrary.com](https://onlinelibrary.wiley.com/doi/10.1002/ldr.4923)]

the mid-20th century position (Figure 2a), is very similar to those of other outlet glaciers of Jostedalbreen, for example, Nigardsbreen (see Winkler, 2021). The rather flat terrain contains numerous moraine ridges of small dimension representing short-term interruptions during the general retreat from the LIA maximum position. The moraines are commonly intersected due to glaciofluvial erosion and large areas of the flat foreland covered by glaciofluvial deposits. Therefore, neither chronologically (Bickerton & Matthews, 1993) nor geomorphologically do the outer forelands provide any indication that Austerdalsbreen's supraglacial debris cover had impacted its length

changes and morphodynamic processes until it retreated into its confined inner valley. Because thick and widespread supraglacial debris cover generally delays response of the glacier terminus to climate warming due to its isolating effect, Austerdalsbreen would not have experienced parallel advance and retreat periods as other (debris-free) Jostedalbreen outlets. Furthermore, the formation of ablation moraines typical for heavily debris-covered glaciers would have resulted in related hummocky terrain rather than defined moraine ridges and the widespread outwash present in Austerdalsbreen's outer foreland. Considerable supraglacial debris on its lower glacier

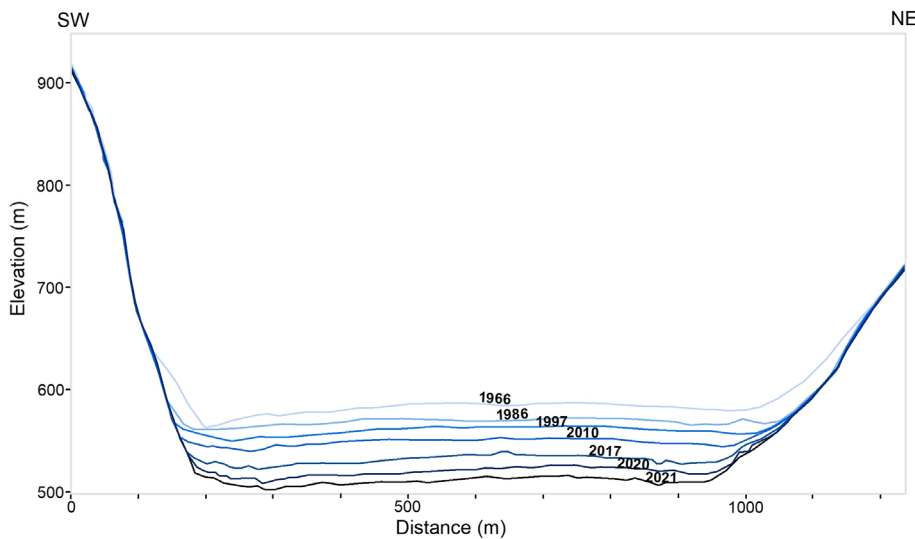


FIGURE 9 Glacier surface elevation along a cross-sectional profile at the central part of Austerdalsbreen (see Figure 8a) at different points in time and adjacent sections of ice-free terrain. Vertical exaggeration is 1.5. [Colour figure can be viewed at [wileyonlinelibrary.com](https://onlinelibrary.wiley.com/doi/10.1002/ldr.4923)]

TABLE 4 Glacier change rates related to surface elevation (Δh) and volume (ΔV). For the respective areas, see Figure 8.

Period of time	Δh (m a ⁻¹)	ΔV (M m ³ a ⁻¹)
1966–1986	-1.4 ± 0.6	~ -3.1
1986–1997	-1.2 ± 1.0	~ -2.6
1997–2010	-1.6 ± 0.8	~ -3.5
2010–2017	-2.6 ± 1.4	~ -5.3
2017–2020	-3.9 ± 1.6	~ -7.1
2020–2021	-10.7 ± 3.0	~ -17.5
2010–2021	-3.6 ± 1.1	~ -5.9
1966–2021	-1.3 ± 0.4	~ -2.9

tongue is specific to Austerdalsbreen compared to other outlet glaciers of Jostedalbreen, which has caused a complex of stagnant ice and debris that has favored the forming of the lake and impacted the overall frontal dynamics during the past decades including the 1990s advance.

The formation of Austerdalsbreen's lake started later than other outlet glaciers of Jostedalbreen. Several outlet glaciers had glacial lake development that occurred within 20 years after a last short readvance culminating around 1930 (e.g., Briksdalsbreen, Bødalbreen, Bøyabreen, Erdalsbreen, and Nigardsbreen; www.nve.no; Laute & Beylich, 2021; Winkler, 2021). Those lakes are partly bound by terminal moraines but mainly occupy pre-existing basins that became ice-free by the glacier retreating upvalley. But, by contrast to Austerdalsbreen, all those glaciers are free of supraglacial debris and temporary may have developed a calving front. But, at no stage, any comparable heavily debris-covered stagnant/dead ice complex was involved. Whereas the lakes at Briksdalsbreen and Erdalsbreen are also located in relatively narrow valleys, the lakes at Bødalbreen, Bøyabreen, and Nigardsbreen occupy central parts within broad foreland terrain. The situation at the lower glacier tongue of Austerdalsbreen is unique for this region.

Both, the rates of glacier surface lowering and the size of the lake of Austerdalsbreen increased after 2010. Notably, the glacial lake's area increased constantly since 2012 (period 2010–2021), whereas the rates of glacier surface lowering were rather constant for decades (since the 1960s) and only increased in recent years, with a slight increase in surface lowering in the period 2010–2017 and a clear increase since 2017 culminating in the last observation period 2020–2021 (Section 5.1.2, Figure 8). Likewise, the glacier volume loss has increased since 2010, whereas the periods before were characterized by rather constant volume loss rates. Another study reveals that three other outlet glaciers of Jostedalbreen (Nigardsbreen, Tunsbergdalsbreen, and Austdalsbreen) had varied surface elevation changes during a similar period from the mid-1960s to ~ 2010 (Andreassen et al., 2020). Surface mass balance also varied between Austdalsbreen and Nigardsbreen for the joint period of observations from 1988 (Andreassen et al., 2020; Andreassen et al., Under review). A comparison of surface elevation changes from 1966 to 2020 for 50 of the outlet glaciers, covering $\frac{3}{4}$ of the total glacier area of Jostedalbreen, shows that Austdalsbreen has a less negative mean elevation change (-0.11 m) than the overall studied part of the ice cap (-0.19 m). This study also finds large inter-variability, for example, Nigardsbreen (-0.06 m), Tunsbergdalsbreen (-0.45 m), and Austdalsbreen (-0.36 m) (Andreassen et al., under review). The increased rates of glacier surface lowering cannot be directly attributed to the recent formation of the glacial lake, however, lake water is seen to favor glacier frontal ablation even though specific local conditions can attenuate or intensify this effect (Truffer & Motyka, 2016). In this regard, relevant factors are thermally induced melting together with thermal undercutting and ponded meltwater beneath and within a glacier (Carrivick & Tweed, 2013; Truffer & Motyka, 2016). This could result in accelerated glacier motion and mass loss, as well as dynamic thinning (Trüssel et al., 2013; Tsutaki et al., 2019), which could introduce positive feedback of increased basal ice motion, reduced effective pressure, and increased flow velocity (Carrivick et al., 2020; Sugiyama et al., 2011).

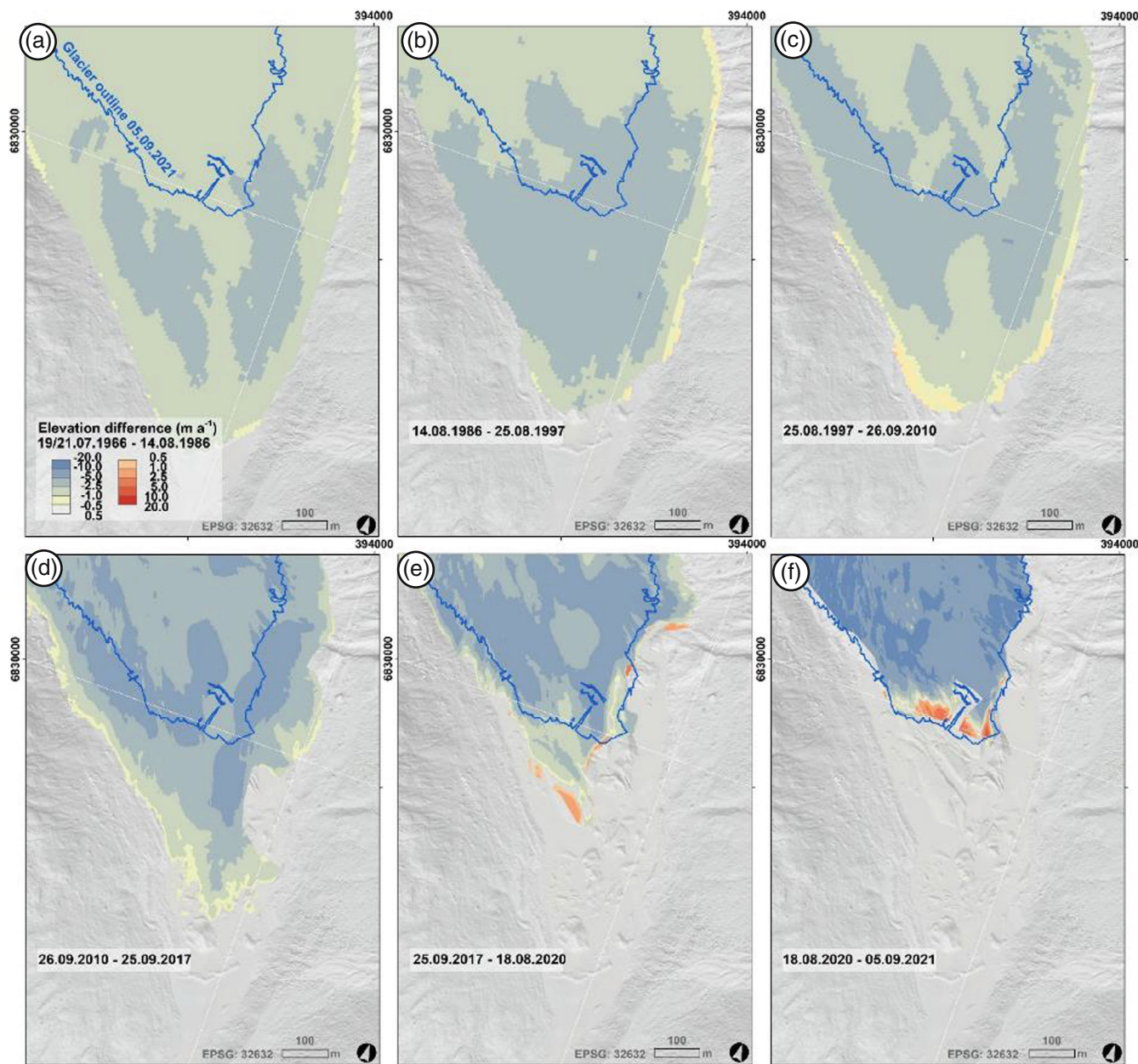


FIGURE 10 Map showing elevation differences and front recession throughout the observation period at the terminus of Austerdalsbreen. [Colour figure can be viewed at wileyonlinelibrary.com]

The constant glacier retreat uncovered the area between the 2021 glacier outline and the moraine ridge of 2000. This moraine ridge is the geomorphic precondition for the formation of the glacial lake, however, it is noticeable that a clear formation and evolution of this lake began 11 years (2012) after the onset of the recession from the moraine ridge but still before the distinct retreat in 2015. As long as this moraine ridge is not affected by erosion due to changing meltwater channels and as long as the glacier retreats, we expect a further increase in the glacial lake. The spatially almost homogeneous glacier surface lowering in the period 2020–2021 at a high level compared to the periods before is an indication of conditions favoring the increase

of the glacial lake. Bedrock conditions below the lowest part of the current margin will determine (and limit) future lake expansion.

7 | CONCLUSIONS

Our results show that the glacier surface at the lower section of Austerdalsbreen has thinned since 1966. The rates of surface lowering have been measured over six subperiods starting in 1966 and increased for each period since the period 1986–1997, with a maximum change rate of $\sim -10.7 \pm 3.0 \text{ m a}^{-1}$ occurring in the last

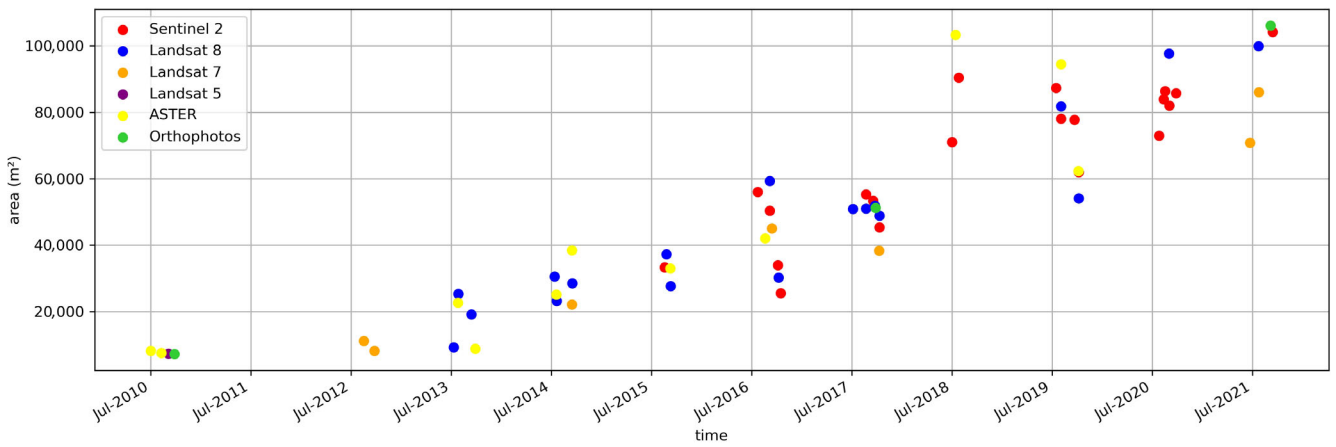


FIGURE 11 Lake area evolution at Austerdalsbreen July 2010–July 2021 based on satellite, airborne, and UAV imagery. [Colour figure can be viewed at wileyonlinelibrary.com]

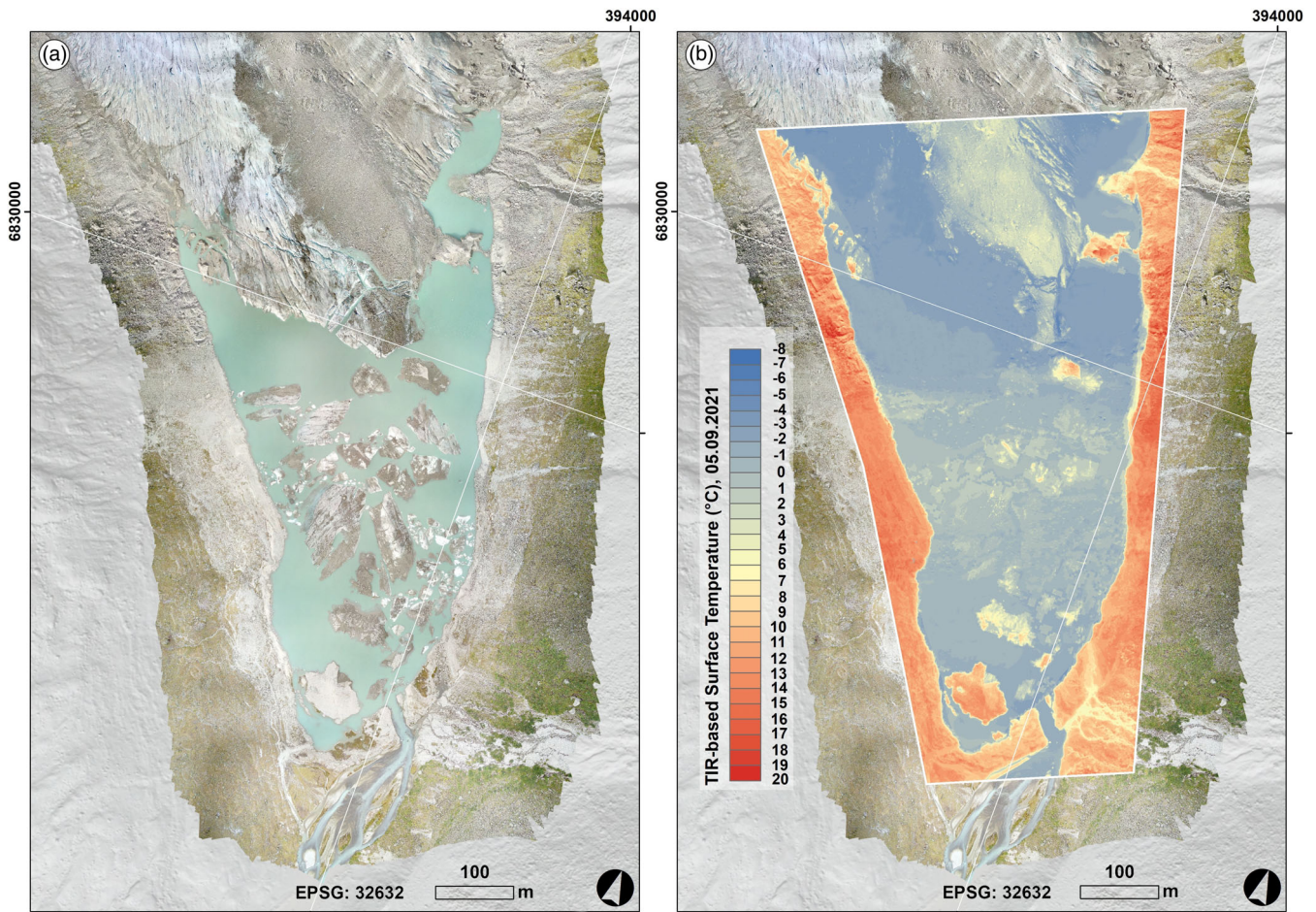


FIGURE 12 UAV-based data acquisition of the frontal part of Austerdalsbreen and its foreland, 05.09.2021 between 16:36 and 16:56 local time: (a) orthophotomosaic and (b) TIR-based surface temperature. [Colour figure can be viewed at wileyonlinelibrary.com]

observation period 2020–2021. While the surface lowering was spatially heterogeneous until 2010, a homogenous lowering appeared in the most recent periods. Favored by a complex of stagnant ice and debris a glacial lake formed that affected the overall frontal dynamics

during the past decades. Since 2012, the area of this moraine-dammed lake considerably increased along the retreating terminus amounting to $\sim 0.1 \text{ km}^2$ in 2021, which likely favors glacier melting and retreat. However, a quantification as to which proportion of the

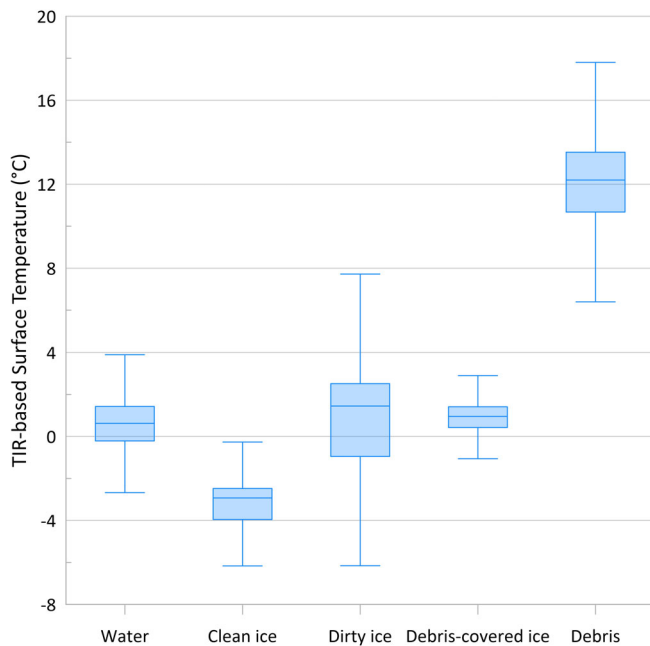


FIGURE 13 Land cover-specific TIR-based surface temperature of the frontal area of Austerdalsbreen, 05.09.2021. [Colour figure can be viewed at [wileyonlinelibrary.com](https://onlinelibrary.wiley.com)]

increased glacier surface lowering and glacier length retreat is attributable to the presence of the recently formed glacial lake is difficult to determine as we showed with the complex interplay of factors during the 1990s advance of the glacier. We found that supraglacial debris on the lower glacier tongue of Austerdalsbreen is specific compared to other outlet glaciers of Jostedalbreen, which contributed to the evolution observed. An in-depth comparison with recent climate trends and the retreat rates of other outlet glaciers of Jostedalbreen could add to our knowledge of the drivers of the observed changes.

ACKNOWLEDGMENTS

Many thanks to the staff of the Tungestølen cabin. We also thank Per Solnes and Marthe Gjerde for permission to use their photographs. We thank review editor José M. Fernández-Fernández for handling the manuscript and two anonymous reviewers for valuable comments that enhanced the manuscript.

FUNDING INFORMATION

This research was part of the JOSTICE project funded by the Norwegian Research Council (project no. 302458).

CONFLICT OF INTEREST STATEMENT

There is no conflict of interest.

DATA AVAILABILITY STATEMENT

The data that support the findings of this study are available from the corresponding author upon reasonable request.

ORCID

Gernot Seier  <https://orcid.org/0000-0003-4790-9425>

REFERENCES

- Abermann, J., Fischer, A., Lambrecht, A., & Geist, T. (2010). On the potential of very high-resolution repeat DEMs in glacial and periglacial environments. *The Cryosphere*, 4(1), 53–65. <https://doi.org/10.5194/tc-4-53-2010>
- Abermann, J., Kuhn, M., & Fischer, A. (2011). Climatic controls of glacier distribution and glacier changes in Austria. *Annals of Glaciology*, 52(59), 83–90. <https://doi.org/10.3189/172756411799096222>
- Abermann, J., Steiner, J. F., Prinz, R., Wecht, M., & Lisager, P. (2020). The red rock ice cliff revisited—six decades of frontal, mass and area changes in the Nunatarssuaq area, Northwest Greenland. *Journal of Glaciology*, 66(258), 567–576. <https://doi.org/10.1017/jog.2020.28>
- Andreassen, L. M., Elvehøy, H., Kjølmoen, B., & Belart, J. M. C. (2020). Glacier change in Norway since the 1960s—an overview of mass balance, area, length and surface elevation changes. *Journal of Glaciology*, 66(256), 313–328. <https://doi.org/10.1017/jog.2020.10>
- Andreassen, L. M., Elvehøy, H., Kjølmoen, B., Engeset, R. V., & Haakensen, N. (2005). Glacier mass-balance and length variation in Norway. *Annals of Glaciology*, 42, 317–325. <https://doi.org/10.3189/172756405781812826>
- Andreassen, L. M., Huss, M., Melvold, K., Elvehøy, H., & Winsvold, S. H. (2015). Ice thickness measurements and volume estimates for glaciers in Norway. *Journal of Glaciology*, 61(228), 763–775. <https://doi.org/10.3189/2015JoG14J161>
- Andreassen, L. M., Nagy, T., Kjølmoen, B., & Leigh, J. R. (2022). An inventory of Norway's glaciers and ice-marginal lakes from 2018–19 Sentinel-2 data. *Journal of Glaciology*, 68, 1085–1106. <https://doi.org/10.1017/jog.2022.20>
- Andreassen, L. M., Robson, B. R., Sjrursen, K. H., Elvehøy, H., Kjølmoen, B., Carrivick, J., & Melvold, K. (Under review). Spatio-temporal variability in geometry changes and geodetic mass balance of Jostedalbreen ice cap. *Annals of Glaciology*.
- Aubry-Wake, C., Baraer, M., McKenzie, J. M., Mark, B. G., Wigmore, O., Hellström, R. Å., Lautz, L., & Somers, L. (2015). Measuring glacier surface temperatures with ground-based thermal infrared imaging. *Geophysical Research Letters*, 42(20), 8489–8497. <https://doi.org/10.1002/2015GL065321>
- Ballantyne, C. K. (2002). Paraglacial geomorphology. *Quaternary Science Reviews*, 21(18–19), 1935–2017. [https://doi.org/10.1016/S0277-3791\(02\)00005-7](https://doi.org/10.1016/S0277-3791(02)00005-7)
- Bennett, M. R., & Glasser, N. F. (2009). *Glacial geology* (2nd ed.). Wiley.
- Bhardwaj, A., Sam, L., Martín-Torres, F. J., & Kumar, R. (2016). UAVs as remote sensing platform in glaciology: Present applications and future prospects. *Remote Sensing of Environment*, 175, 196–204. <https://doi.org/10.1016/j.rse.2015.12.029>
- Bickerton, R. W., & Matthews, J. A. (1993). ‘Little ice age’ variations of outlet glaciers from the Jostedalbreen ice-cap, southern Norway: A regional lichenometric dating study of ice-marginal moraine sequences and their climatic significance. *Journal of Quaternary Science*, 8, 45–66. <https://doi.org/10.1002/jqs.3390080105>
- Bolch, T., Pieczonka, T., & Benn, D. I. (2011). Multi-decadal mass loss of glaciers in the Everest area (Nepal Himalaya) derived from stereo imagery. *The Cryosphere*, 5(2), 349–358. <https://doi.org/10.5194/tc-5-349-2011>
- Brown, M., & Lowe, D. G. (2005). Unsupervised 3D Object Recognition and Reconstruction in Unordered Datasets. 5th International Conference on 3D Digital Imaging and Modeling, Fifth International Conference on 3-D Digital Imaging and Modeling (3DIM'05), Ottawa, Ontario, Canada, June 13–16. <https://doi.org/10.1109/3DIM.2005.81>

- Carrivick, J. L., Andreassen, L. M., Nesje, A., & Yde, J. C. (2022a). A reconstruction of Jostedalbreen during the little ice age and geometric changes to outlet glaciers since then. *Quaternary Science Reviews*, 284, 107501. <https://doi.org/10.1016/j.quascirev.2022.107501>
- Carrivick, J. L., & Heckmann, T. (2017). Short-term geomorphological evolution of proglacial systems. *Geomorphology*, 287, 3–28. <https://doi.org/10.1016/j.geomorph.2017.01.037>
- Carrivick, J. L., How, P., Lea, J. M., Sutherland, J. L., Grimes, M., Tweed, F. S., Cornford, S., Quincey, D. J., & Mallalieu, J. (2022b). Ice-marginal proglacial lakes across Greenland: Present status and a possible future. *Geophysical Research Letters*, 49, e2022GL099276. <https://doi.org/10.1029/2022GL099276>
- Carrivick, J. L., Sutherland, J. L., Huss, M., Purdie, H., Stringer, C. D., Grimes, M., James, W. H., & Lorrey, A. M. (2022c). Coincident evolution of glaciers and ice-marginal proglacial lakes across the southern Alps, New Zealand: Past, present and future. *Global and Planetary Change*, 211, 103792. <https://doi.org/10.1016/j.gloplacha.2022.103792>
- Carrivick, J. L., & Tweed, F. S. (2013). Proglacial Lakes: Character, behaviour and geological importance. *Quaternary Science Reviews*, 78, 34–52. <https://doi.org/10.1016/j.quascirev.2013.07.028>
- Carrivick, J. L., Tweed, F. S., Sutherland, J. L., & Mallalieu, J. (2020). Toward numerical modeling of interactions between ice-marginal Proglacial Lakes and glaciers. *Frontiers. Earth Science*, 8, 577068. <https://doi.org/10.3389/feart.2020.577068>
- DeBeer, C., & Sharp, M. (2009). Topographic influences on recent changes of very small glaciers in the Monashee Mountains, British Columbia, Canada. *Journal of Glaciology*, 55(192), 691–700. <https://doi.org/10.3189/002214309789470851>
- Erikstad, L., & Sollid, J. L. (1986). Neoglaciation in South Norway using lichenometric methods. *Norsk Geografisk Tidsskrift - Norwegian Journal of Geography*, 40(2), 85–105. <https://doi.org/10.1080/00291958608552159>
- Evatt, G., Abrahams, I., Heil, M., Mayer, C., Kingslake, J., Mitchell, S., Fowler, A. C., & Clark, C. (2015). Glacial melt under a porous debris layer. *Journal of Glaciology*, 61(229), 825–836. <https://doi.org/10.3189/2015JG14J235>
- Falatkova, K., Šobr, M., Neureiter, A., Šöner, W., Janský, B., Häusler, H., Engel, Z., & Bene, V. (2019). Development of proglacial lakes and evaluation of related outburst susceptibility at the Adygin ice-debris complex, northern Tien Shan. *Earth Surface Dynamics*, 7(1), 301–320. <https://doi.org/10.5194/esurf-7-301-2019>
- Fraser, C. S. (1996). Network design. In K. B. Atkinson (Ed.), *Close range photogrammetry and machine vision* (pp. 256–281). Whittles Publishing.
- Fugazza, D., Scaioni, M., Corti, M., D'Agata, C., Azzoni, R. S., Cernuschi, M., Smiraglia, C., & Diolaiuti, G. A. (2018). Combination of UAV and terrestrial photogrammetry to assess rapid glacier evolution and map glacier hazards. *Natural Hazards and Earth System Sciences*, 18, 1055–1071. <https://doi.org/10.5194/nhess-18-1055-2018>
- Fyffe, C. L., Brock, B. W., Kirkbride, M. P., Mair, D. W. F., Arnold, N. S., Smiraglia, C., Diolaiuti, G., & Diotri, F. (2019). Do debris-covered glaciers demonstrate distinctive hydrological behaviour compared to clean glaciers? *Journal of Hydrology*, 570, 584–597. <https://doi.org/10.1016/j.jhydrol.2018.12.069>
- Fyffe, C. L., Woodget, A. S., Kirkbride, M. P., Deline, P., Westoby, M. J., & Brock, B. W. (2020). Processes at the margins of supraglacial debris cover: Quantifying dirty ice ablation and debris redistribution. *Earth Surface Processes and Landforms*, 45(10), 2272–2290. <https://doi.org/10.1002/esp.4879>
- Gardelle, J., Berthier, E., Arnaud, Y., & Käab, A. (2013). Region-wide glacier mass balances over the Pamir-Karakoram-Himalaya during 1999–2011. *The Cryosphere*, 7(4), 1263–1286. <https://doi.org/10.5194/tc-7-1263-2013>
- Herreid, S. (2021). What can thermal imagery tell us about glacier melt below rock debris? *Frontiers Earth Science*, 9, 681059. <https://doi.org/10.3389/feart.2021.681059>
- Hirschmüller, H. (2008). Stereo processing by semiglobal matching and mutual information. *IEEE Transactions on Pattern Analysis and Machine Intelligence*, 30, 328–341. <https://doi.org/10.1109/TPAMI.2007.1166>
- Hugonnet, R., McNabb, R., Berthier, E., Menounos, B., Nuth, C., Girod, L., Farinotti, D., Huss, M., Dussailant, I., Brun, F., & Käab, A. (2021). Accelerated global glacier mass loss in the early twenty-first century. *Nature*, 592, 726–731. <https://doi.org/10.1038/s41586-021-03436-z>
- James, M. R., & Robson, S. (2012). Straightforward reconstruction of 3D surfaces and topography with a camera: Accuracy and geoscience application. *Journal of Geophysical Research*, 117(F03017), 1–17. <https://doi.org/10.1029/2011JF002289>
- Kaufmann, V., Kellerer-Pirklbauer, A., & Kenyi, L. W. (2008). Gletscherbewegungsmessung mittels satellitengestützter Radar-Interferometrie: Die Pasterze (Glocknergruppe, Hohe Tauern, Kärnten). *Zeitschr. f. Gletscherkunde u. Glazialgeologie*, 42, 85–104.
- Kaufmann, V., & Seier, G. (2016). Long-term monitoring of glacier change at Gössnitzkees (Austria) using terrestrial photogrammetry. *International Archives of the Photogrammetry, Remote Sensing and Spatial Information Sciences*, 41, 495–502. <https://doi.org/10.5194/isprsarchives-XLI-B8-495-2016>
- King, C. A. M. (1959). Geomorphology in Austerdalen, Norway. *Geographical Journal*, 125, 347–369.
- Kjølmoen, B., Andreassen, L. M., Elvehøy, H., & Storheil, S. (2022). Glaciological investigations in Norway. NVE Rapport 27-2022, 78.
- Kraaijenbrink, P. D. A., Shea, J. M., Litt, M., Steiner, J. F., Treichler, D., Koch, I., & Immerzeel, W. W. (2018). Mapping surface temperatures on a debris-covered glacier with an unmanned aerial vehicle. *Frontiers in Earth Science*, 6, 64. <https://doi.org/10.3389/feart.2018.00064>
- Kraus, K. (1993). *Photogrammetry: Volume 1, fundamentals and standard processes*. Dümmler.
- Krüger, J., & Kjær, K. H. (2000). De-icing progression of ice-cored moraines in a humid, subpolar climate, Kötlujúkull, Iceland. *The Holocene*, 10(6), 737–747. <https://doi.org/10.1191/09596830094980>
- Laute, K., & Beylich, A. A. (2021). Recent glacier changes and formation of new proglacial lakes at the Jostedalbreen ice cap in Southwest Norway. In A. A. Beylich (Ed.), *Landscapes and Landforms of Norway*. World Geomorphological Landscapes. https://doi.org/10.1007/978-3-030-52563-7_4
- Lea, J. M. (2018). The Google earth engine digitisation tool (GEEDiT) and the margin change quantification tool (MaQIT)—Simple tools for the rapid mapping and quantification of changing earth surface margins. *Earth Surface Dynamics*, 6(3), 551–561. <https://doi.org/10.5194/esurf-6-551-2018>
- Lowe, D. (2004). Distinctive image features from scale-invariant keypoints. *International Journal of Computer Vision*, 60(2), 91–110. <https://doi.org/10.1023/B:VISI.0000029664.99615.94>
- Luhmann, T. (2000). *Nahbereichsphotogrammetrie: Grundlagen, Methoden und Anwendungen*. Wichmann.
- Maizels, J. K., & Petch, J. R. (1985). Age determination of intermoraine areas, Austerdalen, southern Norway. *Boreas*, 14, 51–65.
- Nesje, A., Bakke, J., Dahl, S. O., Lie, Ø., & Matthews, J. A. (2008). Norwegian mountain glaciers in the past, present and future. *Global and Planetary Change*, 60, 10–27.
- Nesje, A., & Matthews, J. A. (2011). The Briksdalsbreen event: A winter precipitation-induced decadal-scale glacial advance in southern Norway in the AD 1990s and its implications. *The Holocene*, 22, 249–261. <https://doi.org/10.1177/0959683611414938>
- Nuth, C., & Käab, A. (2011). Co-registration and bias corrections of satellite elevation data sets for quantifying glacier thickness change.

- The Cryosphere, 5(1), 271–290. <https://doi.org/10.5194/tc-5-271-2011>
- NVE. (2022). Norwegian Water Resources and Energy Directorate (NVE). Climate indicator products. <http://glacier.nve.no/viewer/CI/>, downloaded <2022.10.16>
- Østrem, G. (1959). Ice melting under a thin layer of moraine, and the existence of ice cores in moraine ridges. *Geografiska Annaler*, 41(4), 228–230. <https://doi.org/10.1080/20014422.1959.11907953>
- Petch, J. R., & Whittaker, R. J. (1997). Chronology of the Austerdalen glacier foreland. *Zeitschrift für Geomorphologie*, 41, 309–317.
- Pronk, J. B., Bolch, T., King, O., Wouters, B., & Benn, D. I. (2021). Contrasting surface velocities between lake-and land-terminating glaciers in the Himalayan region. *The Cryosphere*, 15(12), 5577–5599. <https://doi.org/10.5194/tc-15-5577-2021>
- Rekstad. (1906). Bræernes framrykning sidsteaar. *Naturen*, 1, Januar 1906, University of Bergen Library. <https://marcus.uib.no/instance/issue/ubb-tnskr-naturen-1906-01.html>
- Robson, B. A., Hölbling, D., Nielsen, P. R., & Koller, M. (2022). Estimating the volume of the 1978 Rissa quick clay landslide in Central Norway using historical aerial imagery. *Open Geosciences*, 14(1), 252–263. <https://doi.org/10.1515/geo-2020-0331>
- Seier, G., Hödl, C., Abermann, J., Schöttl, S., Maringer, A., Hofstadler, D. N., Pröbstl-Haider, U., & Lieb, G. K. (2021). Unmanned aircraft systems for protected areas: Gadgetry or necessity? *Journal for Nature Conservation*, 64, 126078. <https://doi.org/10.1016/j.jnc.2021.126078>
- Seier, G., Kellerer-Pirklbauer, A., Wecht, M., Hirschmann, S., Kaufmann, V., Lieb, G. K., & Sulzer, W. (2017). UAS-based change detection of the glacial and proglacial transition zone at Pasterze Glacier, Austria. *Remote Sensing*, 9, 549. <https://doi.org/10.3390/rs9060549>
- Seier, G., Sulzer, W., Lindbichler, P., Gspurning, J., Hermann, S., Konrad, H. M., Irlinger, G., & Adelwöhrer, R. (2018). Contribution of UAS to the monitoring at the Lärchberg-Galgenwald landslide (Austria). *International Journal of Remote Sensing*, 39, 5522–5549. <https://doi.org/10.1080/01431161.2018.1454627>
- Shean, D. E., Alexandrov, O., Moratto, Z. M., Smith, B. E., Joughin, I. R., Porter, C., & Morin, P. (2016). An automated, open-source pipeline for mass production of digital elevation models (DEMs) from very-high-resolution commercial stereo satellite imagery. *ISPRS Journal of Photogrammetry and Remote Sensing*, 116, 101–117. <https://doi.org/10.1016/j.isprsjprs.2016.03.012>
- Smith, M. W., & Vericat, D. (2015). From experimental plots to experimental landscapes: Topography, erosion and deposition in sub-humid badlands from structure-from-motion photogrammetry. *Earth Surface Processes and Landforms*, 40(12), 1656–1671. <https://doi.org/10.1002/esp.3747>
- Sommer, C., Malz, P., Seehaus, T. C., Lippl, S., Zemp, M., & Braun, M. H. (2020). Rapid glacier retreat and downwasting throughout the European Alps in the early 21st century. *Nature Communications*, 11(1), 3209. <https://doi.org/10.1038/s41467-020-16818-0>
- Stefaniak, A. M., Robson, B. A., Cook, S. J., Clutterbuck, B., Midgley, N. G., & Labadz, J. C. (2021). Mass balance and surface evolution of the debris-covered Miage glacier, 1990–2018. *Geomorphology*, 373, 107474. <https://doi.org/10.1016/j.geomorph.2020.107474>
- Sugiyama, S., Skvarca, P., Naito, N., Enomoto, H., Tsutaki, S., Tone, K., Marinsek, S., & Aniya, M. (2011). Ice speed of a calving glacier modulated by small fluctuations in basal water pressure. *Nature Geoscience*, 4(9), 597–600. <https://doi.org/10.1038/ngeo1218>
- Sutherland, J. L., Carrivick, J. L., Gandy, N., Shulmeister, J., Quincey, D. J., & Cornford, S. L. (2020). Proglacial Lakes control glacier geometry and behavior during recession. *Geophysical Research Letters*, 47(19), E2020GL088865. <https://doi.org/10.1029/2020GL088865>
- Tarca, G., & Guglielmin, M. (2022). Using ground-based thermography to analyse surface temperature distribution and estimate debris thickness on Gran Zebrù glacier (Ortles-Cevedale, Italy). *Cold Regions Science and Technology*, 196, 103487. <https://doi.org/10.1016/j.coldregions.2022.103487>
- Terratec. (2020). Laserskanning for nasjonal detaljert høydemodell. NDH Jostedalsbreen 2pkt 2020. Terratec project. No 10047.
- Terratec. (2021). Rapport for bildematching. Bildedekning: WF-1833 Jostedalsbreen Juli 1966.
- Thomson, L., Brun, F., Braun, M., & Zemp, M. (2021). Editorial: Observational assessments of glacier mass changes at regional and global level. *Frontiers in Earth Science*, 8, 641710. <https://doi.org/10.3389/feart.2020.641710>
- Truffer, M., & Motyka, R. J. (2016). Where glaciers meet water: Subaqueous melt and its relevance to glaciers in various settings. *Reviews of Geophysics*, 54(1), 220–239. <https://doi.org/10.1002/2015RG000494>
- Trüssel, B. L., Motyka, R. J., Truffer, M., & Larsen, C. F. (2013). Rapid thinning of Lake-Calving Yakutat glacier and the collapse of the Yakutat Icefield, Southeast Alaska, USA. *Journal of Glaciology*, 59(213), 149–161. <https://doi.org/10.3189/2013JOG12J081>
- Tsutaki, S., Fujita, K., Nuimura, T., Sakai, A., Sugiyama, S., Komori, J., & Tshering, P. (2019). Contrasting thinning patterns between lake-and land-terminating glaciers in the Bhutanese Himalaya. *The Cryosphere*, 13(10), 2733–2750. <https://doi.org/10.5194/tc-13-2733-2019>
- Ullman, S. (1979). The interpretation of structure from motion. *Proceedings of the Royal Society of London. Series B*, 203(1153), 405–426. <https://doi.org/10.1098/rspb.1979.0006>
- Usamentiaga, R., Venegas, P., Guerediaga, J., Vega, L., Molleda, J., & Bulnes, F. G. (2014). Infrared thermography for temperature measurement and non-destructive testing. *Sensors (Switzerland)*, 14(7), 12305–12348. <https://doi.org/10.3390/s140712305>
- Westoby, M. J., Rounce, D. R., Shaw, T. E., Fyffe, C. L., Moore, P. L., Stewart, R. L., & Brock, B. W. (2020). Geomorphological evolution of a debris-covered glacier surface. *Earth Surface Processes and Landforms*, 45(14), 3431–3448. <https://doi.org/10.1002/esp.4973>
- Winkler, S. (2008). Photographic documentation of front position change at Jostedalsbreen. In B. Kjølmoen (Ed.), *Glaciological investigation in Norway 2007. NVE rapport 2008/1* (pp. 86–87). Norwegian Water Resources and Energy Directorate.
- Winkler, S. (2021). Terminal moraine formation processes and geomorphology of glacier forelands at selected outlet glaciers of Jostedalsbreen, South Norway. In A. A. Beylich (Ed.), *Landscapes and landforms of Norway* (pp. 33–69). (Springer).
- Winkler, S., Elvehøy, H., & Nesje, A. (2009). Glacier fluctuations of Jostedalsbreen, western Norway, during the past 20 years: The sensitive response of maritime mountain glaciers. *Holocene*, 19(3), 395–414. <https://doi.org/10.1177/0959683608101390>
- Winkler, S., & Matthews, J. A. (2010). Observations on terminal moraine-ridge formation during recent advances of southern Norwegian glaciers. *Geomorphology*, 116(1–2), 87–106. <https://doi.org/10.1016/j.geomorph.2009.10.011>
- Winkler, S., & Nesje, A. (1999). Moraine formation at an advancing temperate glacier: Brigsdalsbreen, western Norway. *Geografiska Annaler, Series A: Physical Geography*, 81(1), 17–30. <https://doi.org/10.1111/j.0435-3676.1999.00046.x>
- Yde, J. C., Žárský, J. D., Kohler, T. J., Knudsen, N. T., Gillespie, M. K., & Stibal, M. (2019). Kuannersuit glacier revisited: Constraining ice dynamics, landform formations and glaciomorphological changes in the early quiescent phase following the 1995–98 surge event. *Geomorphology*, 330, 89–99. <https://doi.org/10.1016/j.geomorph.2019.01.012>
- Zemp, M., Frey, H., Gärtner-Roer, I., Nussbaumer, S. U., Hoelzle, M., Paul, F., Haeblerli, W., Denzinger, F., Ahlström, A. P., Anderson, B.,

- Bajracharya, S., Baroni, C., Braun, L. N., Cáceres, B. E., Casassa, G., Cobos, G., Dávila, L. R., Delgado Granados, H., Demuth, M. N., ... Vincent, C. (2015). Historically unprecedented global glacier decline in the early 21st century. *Journal of Glaciology*, 61, 745–762. <https://doi.org/10.3189/2015JoG15J017>
- Zemp, M., Huss, M., Thibert, E., Eckert, N., McNabb, R., Huber, J., Barandun, M., Machguth, H., Nussbaumer, S. U., Gärtner-Roer, I., Thomson, L., Paul, F., Maussion, F., Kutuzov, S., & Cogley, J. G. (2020). Global glacier mass changes and their contributions to sea-level rise from 1961 to 2016. *Nature*, 568(7752), 382–386. <https://doi.org/10.1038/s41586-019-1071-0>

How to cite this article: Seier, G., Abermann, J., Andreassen, L. M., Carrivick, J. L., Kielland, P. H., Löffler, K., Nesje, A., Robson, B. A., Røthe, T. O., Scheiber, T., Winkler, S., & Yde, J. C. (2024). Glacier thinning, recession and advance, and the associated evolution of a glacial lake between 1966 and 2021 at Austerdalsbreen, western Norway. *Land Degradation & Development*, 35(1), 394–414. <https://doi.org/10.1002/ldr.4923>